JOURNAL OF GEOPHYSICAL RESEARCH, VOL. 102, NO. B8, PAGES 18,363–18,390, AUGUST 10, 1997

Integrated log interpretation in the German Continental Deep Drilling Program: Lithology, porosity, and fracture zones

Renate Pechnig, Susanne Haverkamp, and Jürgen Wohlenberg

Lehr- und Forschungsgebiet für Angewandte Geophysik, Rheinisch-Westfälische Technische Hochschule Aachen, Germany

Günter Zimmermann and Hans Burkhardt

Institut für Angewandte Geophysik, Technische Universität, Berlin, Germany

Abstract. Well logs, aquired in the two scientific drill holes of the German Continental Deep Drilling Program (KTB), provide continuous records of physical and chemical data of the metamorphic rocks penetrated. The 4-km-deep pilot hole was almost completely cored, enabling the well logs to be calibrated with regard to rock composition and structural features derived from laboratory analysis of cores. The observed relationships were transferred to the 9101 m deep, nearly uncored, main hole to reproduce in detail the lithology and to estimate physical properties from the logs. Synthetic lithological profiles were constructed for the pilot hole and the main hole by applying the electrofacies concept adapted to the crystalline environment. These profiles provide information on lithostratigraphy, alteration, cataclastic overprint, and petrogenetic features. Cross-hole correlations of these profiles reveal identical rock sequences for large sections of the drilled, metamorphic basement in both holes, in which the primary differences between the protoliths are largely preserved. Multivariate statistical methods were used to determine porosity depth functions from log responses. Linear as well as multilinear regression yielded continuous porosity profiles for both boreholes. Factor analysis was used to extract a parameter interpreted as a fluid and fracture indicator. Comparison of the porosity profiles with lithological information from log, core, and cuttings data revealed two different origins of increased porosity. Rock porosity and permeability are not only related to discrete planar discontinuities such as faults and fractures but also to more extensive zones of intense rock alteration where considerable matrix porosity occurs.

Introduction

The drill site of the German Continental Drilling Program (KTB) is located at the western margin of the Bohemian Massif, the largest surface exposure of crystalline rocks in central Europe (Figure 1). Different structural units of the Variscan orogenic belt are in contact in the vicinity of the KTB drill site. One of the dominant elements is the boundary between the Saxothuringium and the Moldanubium, interpreted as a suture zone of a Variscan, continent-continent collision [*Weber and Vollbrecht,* 1989; *Franke,* 1989]. The drill site itself lies within the Zone of Erbendorf-Vohenstrauss (ZEV), a smaller crustal segment, mainly composed of metabasites and gneisses. Composition and metamorphic evolution under medium-pressure high-temperature conditions (~390 Ma) differ from the low-pressure, high-temperature metamorphism (~320 Ma) of the surrounding Saxothuringium and Moldanubium. To the west of the KTB drill hole the Franconian Line, a large fault zone marking the boundary between the crystalline outcrop of the Bohemian Massif and the Permo-Mesozoic cover of southeast Germany, is the dominant structural element.

Paper number 96JB03802.
0148-0227/97/96JB-03802$09.00

Two boreholes separated by only a short distance from each other were drilled as part of the KTB project. The first drill hole was planned as a pilot hole (KTB-VB, Vorbohrung). It reached a final depth of 4001 m, was almost completely cored, and was extensively logged. It was therefore proposed to drill the main hole (KTB-HB, Hauptbohrung), which was targeted to greater depth, without coring the first 4000 m. Down to the final depth of 9101 m, very few cores were taken. This strategy could only be successful if it were possible to transfer the lithology identified in the pilot hole to the uppermost 4000 m of the main hole and to extrapolate the lithological interpretation down to the final depth.

The reconstruction of the lithological profile of the main well based on cuttings provides only limited depth matching of the petrographical, mineralogical, and geochemical parameters. Similar difficulties are faced when parameters characterizing fluid transport, such as porosity and permeability, are computed for the depth interval of 4000-9101 m of the main well. The only continuous or quasi-continuous information on physical and chemical properties of the pilot hole and the main hole is provided from geophysical borehole measurements. It is therefore reasonable to try to reconstruct the lithological and the hydrological properties within the main hole from an interpretation of geophysical logs. This approach is further justified by the fact that the almost completely cored and logged

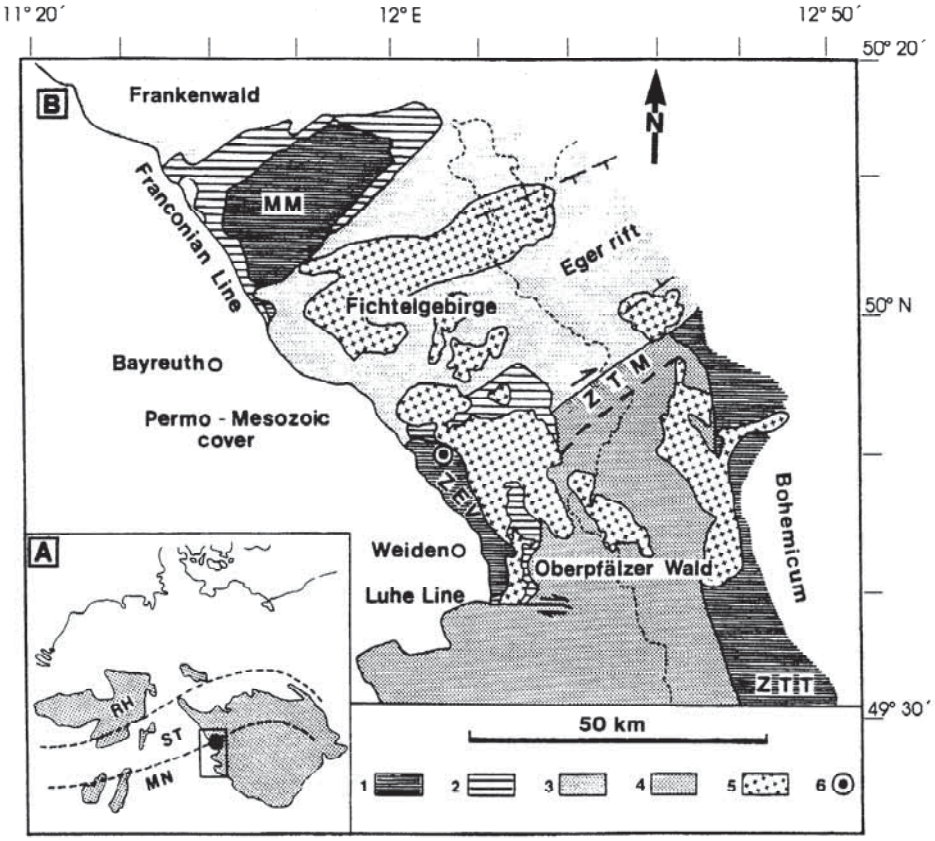

Figure 1. Geological map of the KTB drillsite and vicinity [after *Weber*, 1990]. (a) surface exposure of the Variscan orogenic belt in middle Europe. Distinguished are the three tectono-stratigraphic main units of the Rhenoherzynikum (RH), the Saxothuringikum (ST) and the Moldanubikum (MN). (b) 1, Medium-pressured metamorphic units, comprising the Münchberger Gneismasse (MM), the Zone von Tepla-Taus (ZTT), and the Zone von Erbendorf Vohenstrauss (ZEV); 2, greenshist facies units; 3, Saxothuringikum separated by the mylonitic shear zone Zone von Tirschenreuth Mähring (ZTM) from the 4, Moldanubikum; 5, post-variscian granites; 6, location of the KTB drillsite.

pilot hole provided an excellent opportunity to calibrate the logs with respect to lithology.

Logging data provide information on the composition and on the structural features of the drilled rock. While logging data has been utilized for decades by the oil industry in sedimentary environments [*Serra*, 1984, 1986; *Ellis*, 1987], only little was known about the use of such data for lithological determination or investigations of in situ physical properties (e.g., porosity, permeability) of crystalline basement rocks, when KTB was initiated in 1987. More recently, investigations have been conducted in this field, especially in exploration wells for mineral mining, geothermal energy or radioactive waste deposits [*Sattel*, 1986; *Paillet*, 1991; *Nelson and Johnston*, 1994], as well as in the framework of research drillings in continental or oceanic crust [e.g., *Broglia and Moos*, 1988; *Pezard*, 1990; *Moos*, 1990; *Anderson et al.*, 1985; *Goldberg et al.*, 1991; *Daniels et al.*, 1983; *Pratson et al.*, 1992; *Anderson et al.*, 1990]. These studies have shown that the complex geological conditions of crystalline rocks, particularly metamorphics, are not easily determinable from the logs. Traditional interpretation techniques often lead to ambiguous or erroneous results because of the strong superposition of log responses produced by the varying composition and structural variations of crystalline rocks. Hence reliable log interpretation in crystalline basement requires an integrated approach, using both logs and information from rock samples. The KTB project thus provided an outstanding opportunity to reconcile downhole data with the petrographical and petrophysical features of crystalline rocks.

The objectives of analyzing the logging data presented in this paper are twofold: The first part of the paper deals with the reconstruction of the lithology [*Haverkamp*, 1991; *Haverkamp and Wohlenberg*, 1991; *Pechnig*, 1996], which involves the identification of rock type and associated specific mineralogical and geochemical properties, and the detection of altered and cataclastic overprinted depth sections. The second part of the paper focuses mainly on the petrophysical properties of the crystalline crust. In this case, the logging data were used to estimate the porosity of the drilled rocks [*Zimmermann et al.*, 1992b]. It is important to map porosity because it is closely related to permeability, fluid movements, and heat transport in continental crust. In both cases, the interpretation concepts developed were divided into two stages. In the first stage, the logging data were calibrated by comparing them with the mineralogical, geochemical, and petrophysical data from cores retrieved from the pilot hole. In the second phase, relationships between rocks and log responses found in the pilot hole were transferred to the main hole to construct continuous lithology

Table 1. Acronyms and Full Names of All Tools and Logs Used for the Presented Interpretation

Tool	Log		Principle
DLL (Dual LateroLog)	LLD (ohm m)	laterolog deep	electrical resistivity
	LLS (ohm m)	laterolog shallow	
	MSFL (ohm m)	microspherical focused log	
SDT (Sonic Digital Tool)	DTCO (μs/m)	compressional wave travel time	travel time of sound
	DTSM (μs/m)	shear wave travel time	
DSI (Dipole Shear Sonic Imager)	DTST (μs/m)	stoneley wave travel time	
CNT (Compensated Neutron Tool)	NPHI (p.u.)	neutron porosity	absorption of neutrons
LDT (Litho Density Tool)	RHOB (g/cm^3)	bulk density	absorption/scattering of γ rays
	PEF (barns/el)	photoelectric effect	
GLT (Geochemical Logging Tool)			
AACT (Aluminium Activation Clay Tool)	WAL (%)	aluminium content	neutron-activated γ ray emissions
GST (Induced Gamma Ray Spectrometry Tool)	WCA (%)	calcium content	neutron-activated γ ray emissions
	WFE (%)	iron content	
	WSI (%)	silicium content	
	WTI (%)	titanium content	
	WGD (ppm)	gadolinium content	
	CSIG (c.u.)	neutron capture cross section	
NGT (Natural Gamma Spectrometry Tool)	SGR (API)	spectral (total) gamma ray	natural γ ray emissions
	POTA (%)	potassium content	
	THOR (ppm)	thorium content	
	URAN (ppm)	uranium content	

API American Petroleum Institute, c.u. capture units, p.u. limestone porosity units

and structure profiles of the uncored sections using solely the logs.

Log and Laboratory Data

A wide spectrum of logging operations was carried out within the pilot hole and the main hole, including the recording of acoustic, electric, nuclear, geochemical, magnetic, and borehole imaging data [*Draxler*, 1990; *Bram et al.*, 1991; *Bram and Draxler*, 1992, 1993, 1994]. The logs which have been evaluated for this study (Table 1) are spectral (total) gamma ray (SGR), potassium (POTA), thorium (THOR), uranium (URAN), density (RHOB), photoelectric effect (PEF), neutron porosity (NPHI), sonic (DTCO, DTSM, DTST), resistivity (LLD, LLS, MSFL), caliper (CAL), and some main and trace elements (WSI, WCA, WFE, WAL, WTI, WGD), which were recorded with the geochemical logging tool. These logs were recorded over the entire length of the pilot hole, but their use was limited within the main hole, where the extremely large bit size used to drill the upper 3 km (44.5 cm), the increasing temperatures and the rather poor well bore conditions in the deeper sections meant that the logging program had to be strongly reduced. An overview of logging operations which were undertaken in the pilot hole and the different depth sections of the main hole is given in Figure 2.

Extensive data from cores, cuttings, rock flour, drilling fluids, and gases from the pilot hole and the main hole were collected by the KTB Field Laboratory [*Umsonst et al.*, 1995]. Initial petrographical descriptions, thin section examinations [*Röhr et al.*, 1990, *Duyster et al.*, 1995], X ray fluorescence and X ray diffraction analyses [*Stroh et al.*, 1990; *Machon*, 1995], and a wide spectrum of measurements to determine physical properties, such as seismic, electrical, and magnetic parameters, were carried out routinely. A complete listing of the petrophysical data sets and their interpretation with respect to rock composition and structure are given by *Berckhemer et al.* [this issue]. Laboratory investigations were performed predominantly on cores from the pilot hole. In the main hole, only 35 core runs were carried out, with a total core recovery of 83.34 m. Here, cuttings were analyzed routinely in intervals between 0.5 and 10 m.

Quality of Logging Data

Accuracy of logging data is most important for a reliable interpretation and extensive quality controls were therefore carried out. The processing was as follows: First, standard borehole corrections were performed on the logs to compensate for the effects of drilling fluids, bit size variations and logging speed changes [*Gatto*, 1992]. The raw geochemical data sets retrieved by natural γ ray spectroscopy (POTA) and neutron-activated γ ray spectra (WAL, WSI, WFE, WCA, WTI) were transformed into dry weight percentages of the elements [*Gatto*, 1993]. The procedure was carried out using a model calculation developed specifically for geochemical logging [*Schweitzer et al.*, 1988; *Grau and Schweitzer*, 1989]. Once processed in this way and integrated as a depth matched composite log, the data were ready for interpretation.

Before the following log analyses were performed, data were checked for accuracy, with the logs being compared with geochemical and petrophysical measurements on cores and cuttings, respectively. In the pilot hole, differences between core and logging depths, caused by weight and buoyancy of the probes and the lengthening of the drill pipe, had to be corrected. Systematical depth differences (about 1 m deviation per 1000 m depth) were identified and corrected for in the pilot hole by the

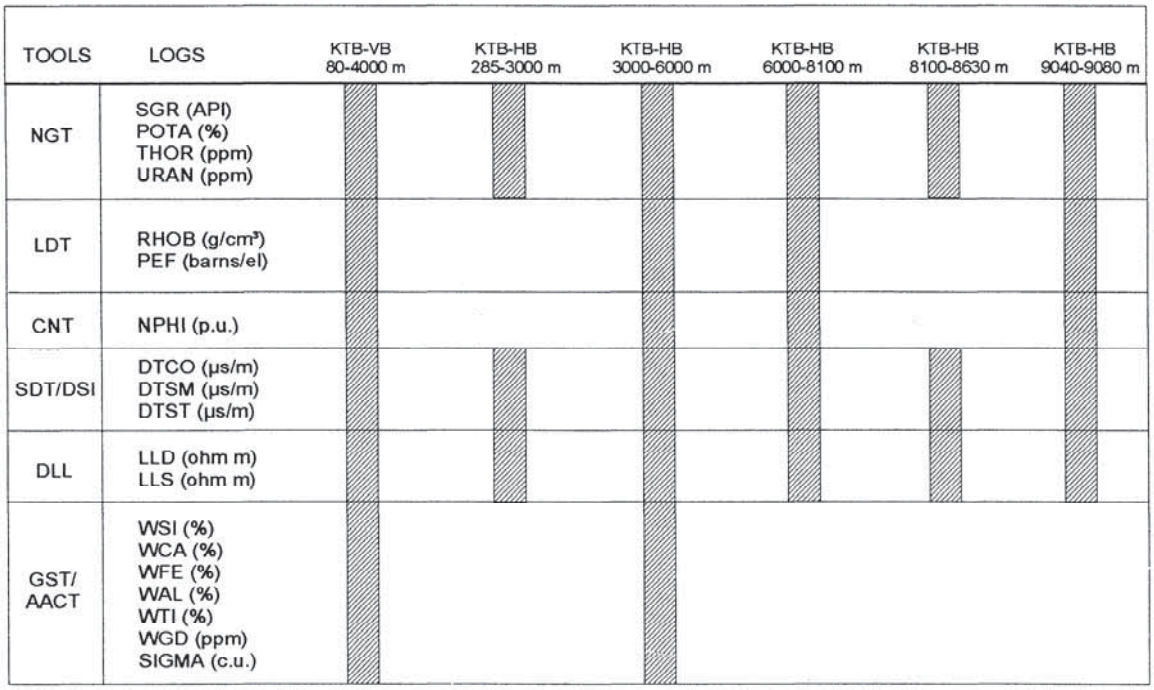

Figure 2. Logs obtained in the pilot hole (KTB-VB) and in the main hole (KTB-HB).

use of autocorrelation methods [*Zimmermann et al.*, 1992a] comparing core and log γ ray measurements. Systematic differences between log and cuttings data due to depth were not observed in the main hole. Differences occur unsystematically and can extend more than 10 m. Figures 3a and 3b show logs for the pilot hole and the main hole compared to core and cuttings data, respectively. In general, the correlation is very good. This is especially the case for the density and the γ ray measurements. Depth resolution of logging data is between that of distinct core data and that of strongly mixed cuttings data. Although the geochemical parameters displayed are highly correlated, minor systematic deviations were observed and taken into account for further interpretation. These deviations were mostly observed between single runs and might be caused by preprocessing and data corrections due to bitsize and mud environment.

Records of electrical and seismic borehole measurements could not be checked for accuracy by comparison with core data, as was possible for the neutron and γ logs, because the strong anisotropy of the rocks created by their pronounced metamorphic fabric gives rise to larger deviations between the in situ logs and the laboratory data [*Siegesmund et al.*, 1993; *Berckhemer et al.*, this issue].

Severe borehole breakouts occur frequently in the KTB boreholes, especially in the deeper parts of the main well [*Borm et al.*, this issue]. These breakouts effect data accuracy. This is especially the case for the density log (Figure 3b), while elemental logging is not so strongly influenced. Only the aluminium measurement is more sensitive to breakouts due to the lower activation energy used by the AACT. The sonic logs, as well as the neutron porosity, were affected mainly by the rugosity of the borehole wall. Electrical devices with small penetration depth (MSFL, LLS) also show strong dependence on borehole conditions, which is not the case for the LLD. Considering this different influence on log responses, data of caved sections were checked for reliability, and in some sections, logs were excluded from further interpretation.

Reproduction of Lithology

All rocks penetrated in the KTB main and pilot hole belong to one tectono-metamorphic unit, the Zone of Erbendorf-Vohenstrauss (ZEV). The metamorphic rocks, overprinted under medium pressure conditions [*O'Brien et al.*, this issue], can be subdivided into three lithological associations of (1) paragneiss sections derived from turbiditic greywackes, (2) massive metabasitic units of igneous origin with enriched mid-ocean ridge basalt (MORB) characteristic, and (3) varied units of partly calc-silicate bearing paragneiss-metabasites alternations of former volcano-sedimentary sequences. These three main lithological units with thickness ranging from 100 to 1000 m are, more or less, repeated until the final depth of the main well of 9101 m (Figure 4). The whole section is characterized by steeply dipping foliation (50-70°), predominantly in a SW direction, and abundant fault zones resulting from multistage brittle deformation. The most important fault zone was transected between 6850 and 7260 m depth in the main hole. This steeply dipping discontinuity, which belongs to the fault system of the Franconian Lineament [*Hirschmann and Lapp*, 1994], could be linked to the most prominent reflection (SE1) revealed by surface seismics [*Harjes et al.*, this issue].

The aim of our investigation was to transform recorded log responses into lithological terms and thus construct a detailed and correct, depth-integrated, lithological profile for the mostly uncored main well deduced only from the logs. Since there was not much experience concerning the identification of crystalline rocks from logs when KTB started, reliable interpretation techniques had first to be developed and tested.

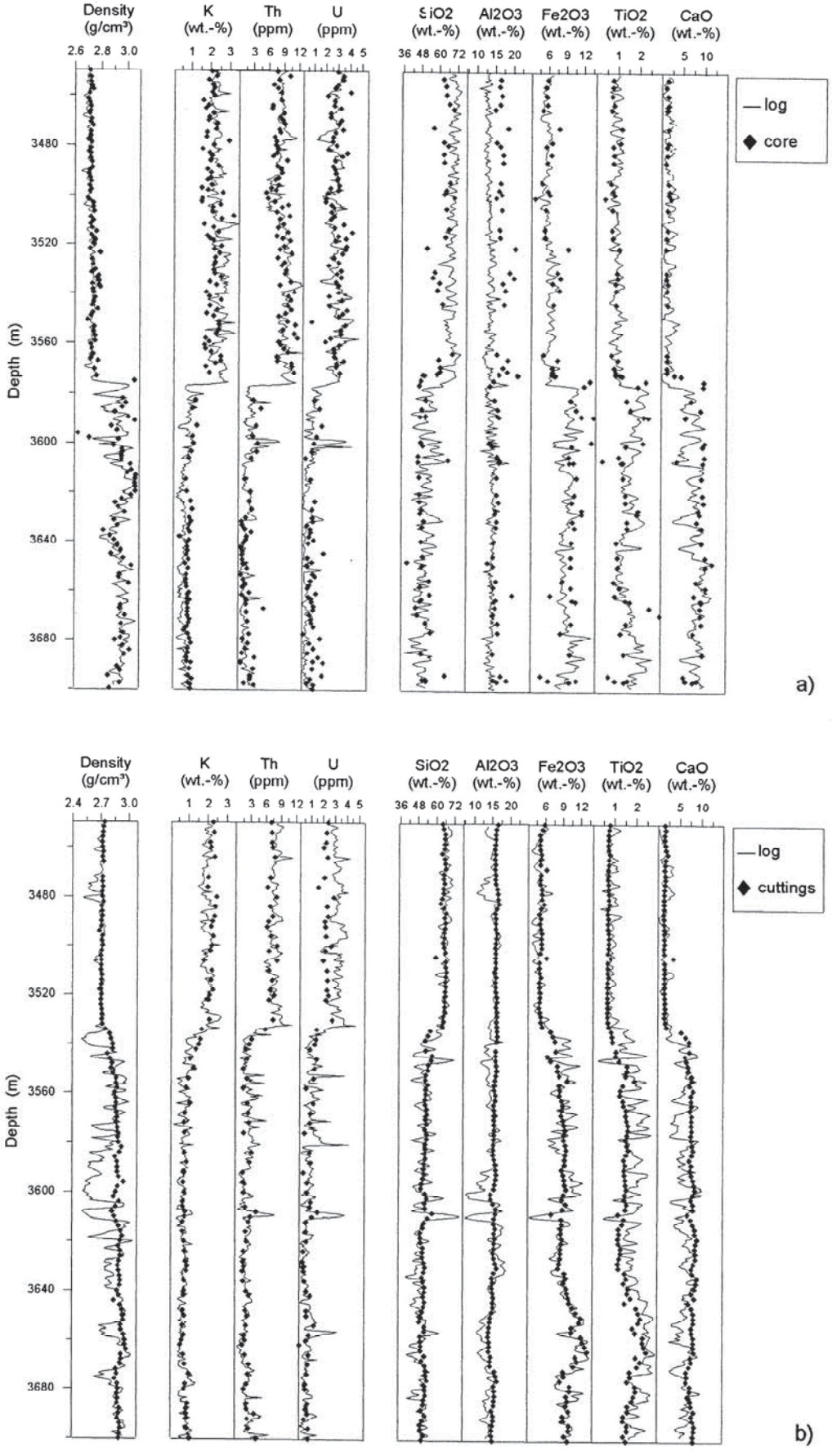

Figure 3. Logs compared to (a) core and (b) cuttings measurements from the pilot hole and from the main hole, respectively. Displayed are logs retrieved by the LDT, NGT, GST, and AACT. The chemical logs are calculated as oxides using the factors from the metamorphic model [*Schweitzer et al.*, 1988].

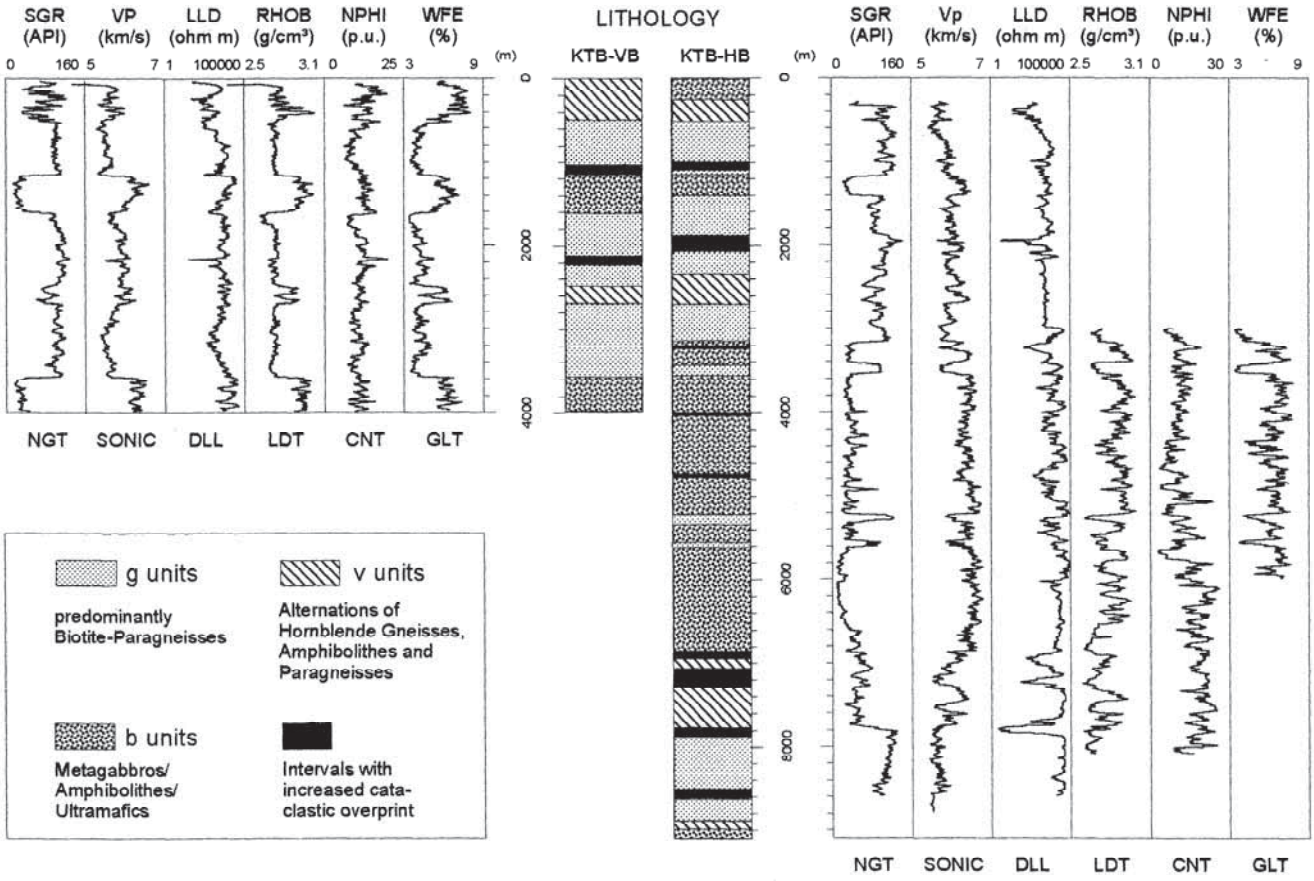

Figure 4. Overview of the lithology drilled through in both boreholes compared to some logs (one of each tool). Shown is a simplified lithological profile, where only the main lithological units are marked: paragneiss units (g units), metabasitic units (b units), and varied units (v units). Logging data are resampled to 1m and smoothed by a 21-point sliding window. Full names of acronyms used for the logs and tools are given in Table 1.

EFA-Log Evaluation Concept

The interpretation technique [*Haverkamp and Wohlenberg*, 1991] considers all information available from logging and investigations on rock samples in order to calibrate the logs with the lithology. This calibration was performed preferably on the cored sections of the pilot hole. Basically, information on the drilled lithological profile come from the petrographic descriptions carried out in the Field Laboratory [see *Röhr et al.*, 1990; *Lich et al.*, 1992; *Duyster et al.*, 1993, 1995]. In addition, geochemical and mineralogical data, as well as petrographical thin section analyses, were used to obtain more detailed information about the quantitative mineral content, the chemical signature, and the alteration. Integrating this information resulted in qualitative and quantitative definitions of the lithological characteristics of each rock type.

To derive the relations between these lithological characteristics and the recorded log responses, data were displayed as two- or three-dimensional cross plots. Besides the distinct separation of the main lithological units, trends reflect the dependence of the tool responses on the mineralogical/geochemical variations and on structural changes of the rocks. Thus they are helpful in calibrating the logs in so far that definite log values can be assigned to certain lithological characteristics. These characteristics might be defined by the quantitative mean mineralogical composition of the rock type, by chemical signatures, by the occurrence of rare but conspicuous mineral assemblages (e.g., radioactive accessories, ore minerals), or by specific structural features like fissuring or faulting. So, step by step, each lithotype revealed by drilling will be classified by an individual set of tool responses, the so-called electrofacies [*Serra*, 1986]. Each electrofacies comprises the definite ranges of all log values for the corresponding lithological unit and differs from all the others in at least one parameter. This procedure was carried out predominately in cored calibration sections of the pilot hole.

Once the electrofacies are defined, they can be transferred to unknown depth sections or other boreholes, in this case to the main well. This transfer was performed by the use of statistical methods included in the Western Atlas "HORIZON" software package. With this program, developed by *Tezlaff et al.* [1989], qualitative variables such as lithologies can be estimated from the logging data. The variable to be estimated must be well known in one or more depth intervals, which is the case in the pilot hole. The program consists of two processing modes: In a first step the program "learns" the correspondence between the variable (lithology defined by the electrofacies) and the set of estimators (logging data) in these known intervals then uses this knowledge to infer the estimated variable where only the estimators are known.

The computational mechanics are as follows. First, data from calibrated sections are stored into a database. This database can be imagined as a multi dimensional cross plot. The dimension of this cross plot is dependent on the number of estimators

(logs) used. The range of each log is divided into steps, from which single cells are constructed. Each depth level in the training set produces one data point that falls into one of these cells. The frequency of points and their respective electrofacies are stored for each cell. Hence the distribution density of each user defined category (electrofacies) can be estimated from the distribution of the points of the training set. Before any estimation is made, the constructed database must be checked for quality. Robustness and discrimination power are tested by the calculation of discrimination matrices for the user defined categories (electrofacies). The user can optimize the previously defined subdivision of the training section by repeating this procedure several times. Using the complete logging suite, 37 electrofacies, each one corresponding to one distinct lithotype, could be successfully stored and differentiated in the pilot hole. This database was supplemented in the main hole by the definition of eight new electrofacies.

In the "query" mode, the logging data of unknown depth sections are compared with the multidimensional database, and the most probable lithotype is assigned level by level. Probabilities are obtained from estimator distribution by applying Bayes theorem:

$$p(A_i \mid X) = \frac{f_i(X)\, p(A_i)}{\sum_{j=1}^{m} [f_j(X)\, p(A_j)]}$$

where

p	probability function;
A_i, A_j	categories (electrofacies i,..,j);
m	number of categories;
X	vector containing the values of the estimators (logs);
$p(A_i \mid X)$	probability that category A_i is present at a depth level given the set of estimators X;
f_i, f_j	statistical distribution densities of the estimators for each category.

Thus a confidence value is given for each level. If a new, hitherto unknown lithotype is transected and log responses of this section do not match with one from the stored categories, the calculated probability tends to zero. In this case, the log responses of this unknown type are calibrated and added to the database as described above. By repetition, this procedure leads finally to the generation of a synthetic lithological borehole profile, the EFA-log (electrofacies-log).

General Relation of Log Responses to Rock Composition

The main rock types observed in cores and cuttings are different varieties of biotite-plagioclase paragneisses, amphibolites, metagabbros, and hornblende gneisses. Subordinate potassium-feldspar gneisses and ultramafics are intercalated. Postorogenic lamprophyres and aplites crosscut the entire section. An overview of these most important rock types is given in Table 2. The complete log response ranges of their corresponding electrofacies are displayed in Figure 5. In addition to these main rock types, various subtypes could be characterized and separated by their log responses. Some of them are also listed in Table 2. Considering all occurring mineralogical and chemical subvarieties of the rocks (only the most important types are mentioned in this paper), as well as rock types changed by alteration or cataclastic overprint, in all, more than 40 different lithotypes were distinguished in both boreholes, each one defined by an individual electrofacies [*Haverkamp*, 1991; *Pechnig*, 1996]. Petrographical descriptions, mean mineralogical composition, and electrofacies data limits for all lithotypes are available on request.

Mineralogical-chemical composition and physical properties of the most important rock types, which are listed in Table 2, are sufficiently different from one another to be clearly distinguishable by means of the logs. The most important parameter for differentiating the metamorphic succession is the total γ ray (SGR). Owing to the chemical composition, γ activity exhibits a general increase from the most mafic rocks (ultramafitites) to the most acidic rocks (potassium-feldspar-gneisses) observed in the boreholes (Plates 1a-f). With regard to rock composition, the variation of the γ log can be linked to the other logging parameters as described in the following text.

In general, amphibolites and metagabbros, which are the main rock types of the massive metabasite units, are physically characterized by lower gamma activity and higher density than the rocks of the paragneiss sections (Plate 1a). This is related to mineral content which, within the metabasites, consists of more mafic and dense minerals like hornblende and garnet biotite than in the paragneisses, which are composed mainly of quartz, plagioclase, and micas. The more mafic chemical composition of the metabasites is reflected by much lower silicon and potassium (Plate 1b) concentrations and by increased iron values (Plate 1d). Regarding these general trends, which are related to the amount of felsic to mafic mineral components of the rocks, hornblende gneisses, ranked between amphibolites and paragneisses in composition, are consequently characterized by intermediate log responses (Plates 1a, 1b, and 1d). Owing to the higher potassium content, the highest gamma activity is recorded in the potassium-feldspar-gneisses, with maximum values of up to 200 API (Plate 1b). Further, these quartz-and plagioclase-rich rocks show the lowest density values (Plate 1a) and are characterized geochemically by very high aluminium values, bound to the feldspar minerals (Plate 1d). This relation between the aluminum content and amount of feldspar minerals is also responsible for the low aluminium values recorded in the ultramafitites, which are almost free of feldspar.

The recorded neutron porosity (NPHI), sensitive to the total water content of the formation, is also dependent upon mineralogical composition, since pore space in the crystalline basement is mostly very low. Enhanced porosity is in general restricted to discrete zones of faulting and fracturing, and NPHI in undisturbed depth sections is predominantly reacting to the water content bound in minerals like phyllosilicates or amphiboles. Hence rock types poor in these minerals, such as quartz and feldspar-rich gneisses show very low neutron porosities. In contrast, rocks with high phyllosilicate and amphibole contents produce striking increases in the NPHI log. In addition to the lamprophyres, this is especially the case for the ultramafitites, which consist on average of more than 80% hornblende, chlorite, and serpentinite (Plate 1c). Increased chlorite contents also occur in the gneisses, amphibolites, and metagabbros as a consequence of retrograde overprint. Thus NPHI is also useful as an indicator for the grade of alteration.

The sonic records of transit travel times of compressional (DTCO) and shear waves (DTSM) are also strongly affected by rock composition. In general, sonic travel time decreases with increasing density and consequently with the amount of mafic minerals (Plate 1e). Significant differences were determined

Table 2. The Most Important Rock Types and their Subtypes Drilled in the KTB Holes

Rock Type	Litho Unit	Occurence	Main Electrofacies Characteristic	Subtypes	significant limits
			Gneisses		
Biotite-paragneiss (dominant rock type of the paragneiss-units)	g, v	*	SGR 70-130, POTA 1.0-3.5, RHOB 2.65-2.85, NPHI 5-15, DTCO 170-200, WFE 3.0-5.7	mica-rich quartz-rich very quartz-rich	SGR > 100, POTA > 2.7 SGR < 100, RHOB < 2.75 SGR < 85, NPHI < 9
Hornblende gneiss (dominant rock type of the varied units)	v, b, g	+	SGR 40-90, POTA 1.0-2.6, RHOB 2.65-2.9, NPHI 1-15, DTCO 155-180, WFE 3-8	foliated type, biotite-rich (sedimentary origin in v,g units) augengneiss, plagioclase-rich (magmatic origin, occur only in b units)	SGR > 60, THOR > 4, RHOB > 2.75 SGR < 65, RHOB < 2.75, WFE < 5
Potassium-feldspar gneiss	only in v	#	SGR 120-190, POTA 3-8, RHOB 2.6-2.75, NPHI 0-9, WAL 8-12, WFE 2.5-7.5		
			Metabasites		
Amphibolite (dominant rock type of the metabasitic units)	b, v	*	SGR 20-50, POTA 0-1.5, RHOB 2.75-3.1, NPHI 5-20, DTCO 150-175, WFE 5-10	massive type, hornblende-garnet-rich partly with qrz-fsp-mobilisates rich in qrz-fsp-mobilisates	RHOB > 2.93, WFE > 6 RHOB 2.85-2.93 RHOB < 2.85, WFE < 6
Metagabbro	only in b	+	SGR 0-20, POTA 0-1, THOR 0-3, WFE 4-13, RHOB 2.9-3.15, DTCO 140-170	normal MORB-type primitive chemical signature highly fractionated, garnet-rich	WAL < 9, WFE < 9.5 WAL > 8.5, WFE < 6.5 WFE > 9.5
Ultramafitite	only in b	§	SGR 0-20, POTA 0-0.7, RHOB 2.9-3.15, NPHI 15-30, WFE 7-12, WAL 3-6		
			Dikes		
Aplite	crosscut b, g, v	§	SGR 90-150, POTA 2-5, THOR 8-20, WFE 2.5-5		
Lamprophyre		#	SGR 90-130, RHOB 2.7-2.8, NPHI 15-23, WFE 3-7		

The main electrofacies ranges and the significant limits for distinguishing the various subtypes are given. Quartz, qrz; feldspar, fsp.
* Very frequently.
+ Frequently.
# Rare.
§ Very rare.

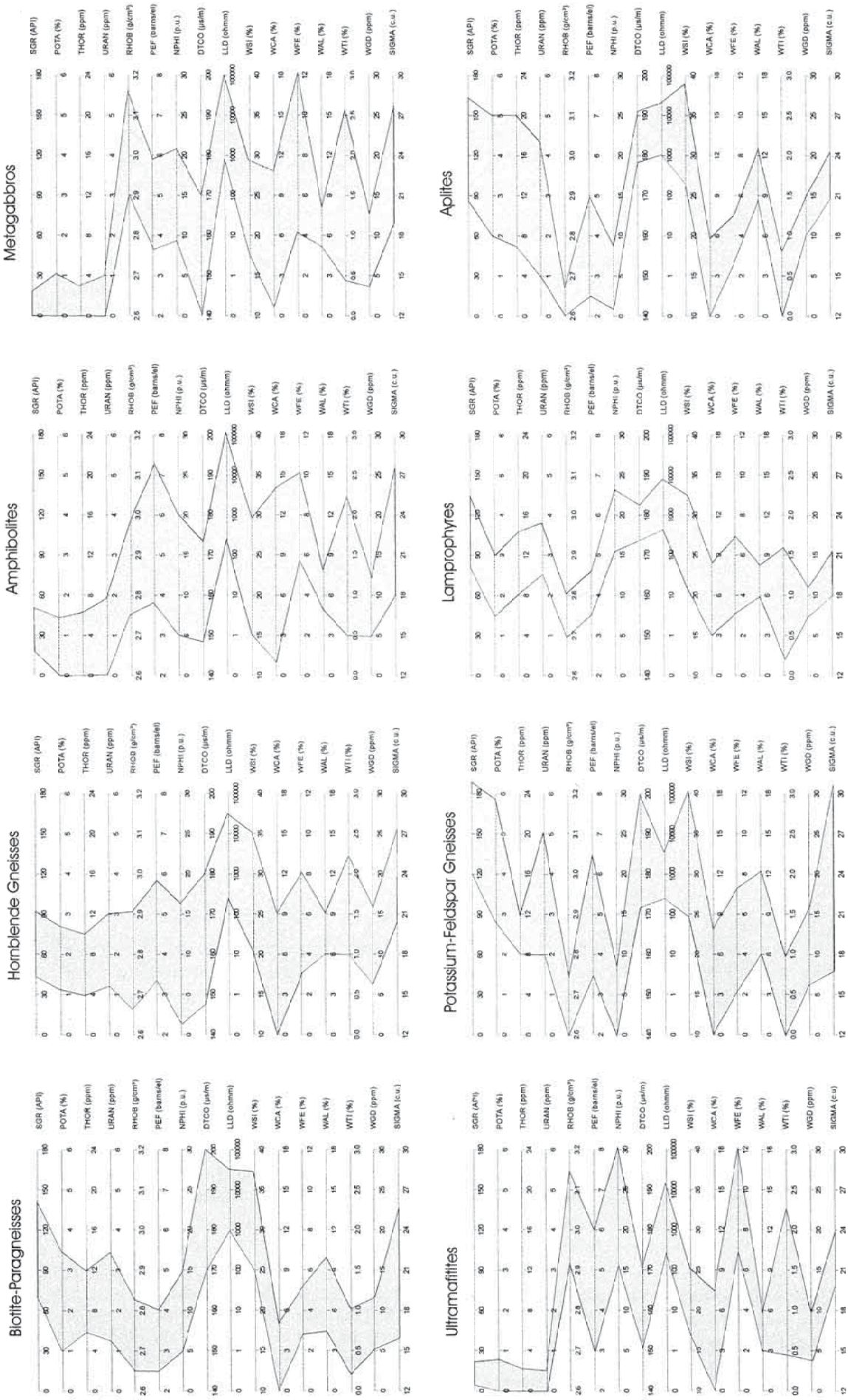

Figure 5. Electrofacies diagram for the main rock types of biotite-plagioclase-paragneisses, hornblende gneisses, amphibolites, and metagabbros and for the minor occurring rock types of metaultramafics, potassium-feldspar-gneisses, lamprophyres, and aplites.

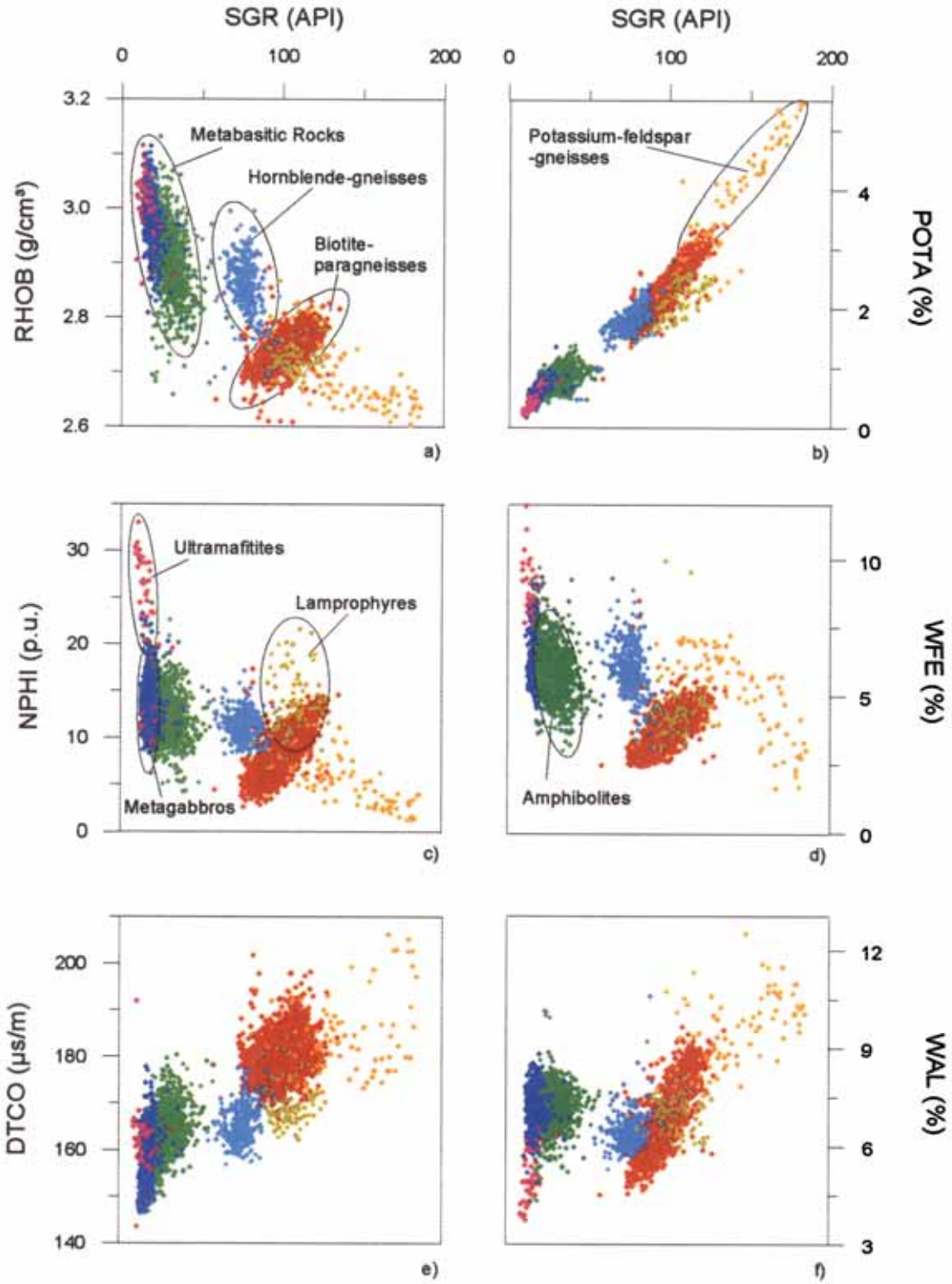

Plate 1. Main rock types reflected by cross plots of the logs SGR versus (a) RHOB, (b) POTA, (c) NPHI, (d) WFE, (e) DTCO, (f) WAL. Data from calibration sections of the pilot hole are displayed: 600-900 m, paragneisses; 1200-1400 m, metabasitic unit of amphibolites, metagabbros, and ultramafics; 2400-2600 m, hornblende gneisses. Data for the potassium-feldspar-gneisses are obtained from the varied unit between 0 and 480 m. Data for lamprophyres are selected from the entire depth section. Data are selected only if caliper is within 4 cm of bit size.

between the travel times in metabasites, with average values of ~160 µs/m (DTCO), and those in paragneisses, ranging between 165 and 200 µs/m (DTCO). Since physical log records, such as density and sonic travel time are strongly dependent on well bore conditions and structural features of the rocks, these logs are reliable for lithology detection only in tectonically undisturbed and rather uncaved borehole sections.

Whereas the physical and chemical logs mentioned above are strongly affected by rock composition, this is not the case for the electrical logs. Resistivity values are generally very high in

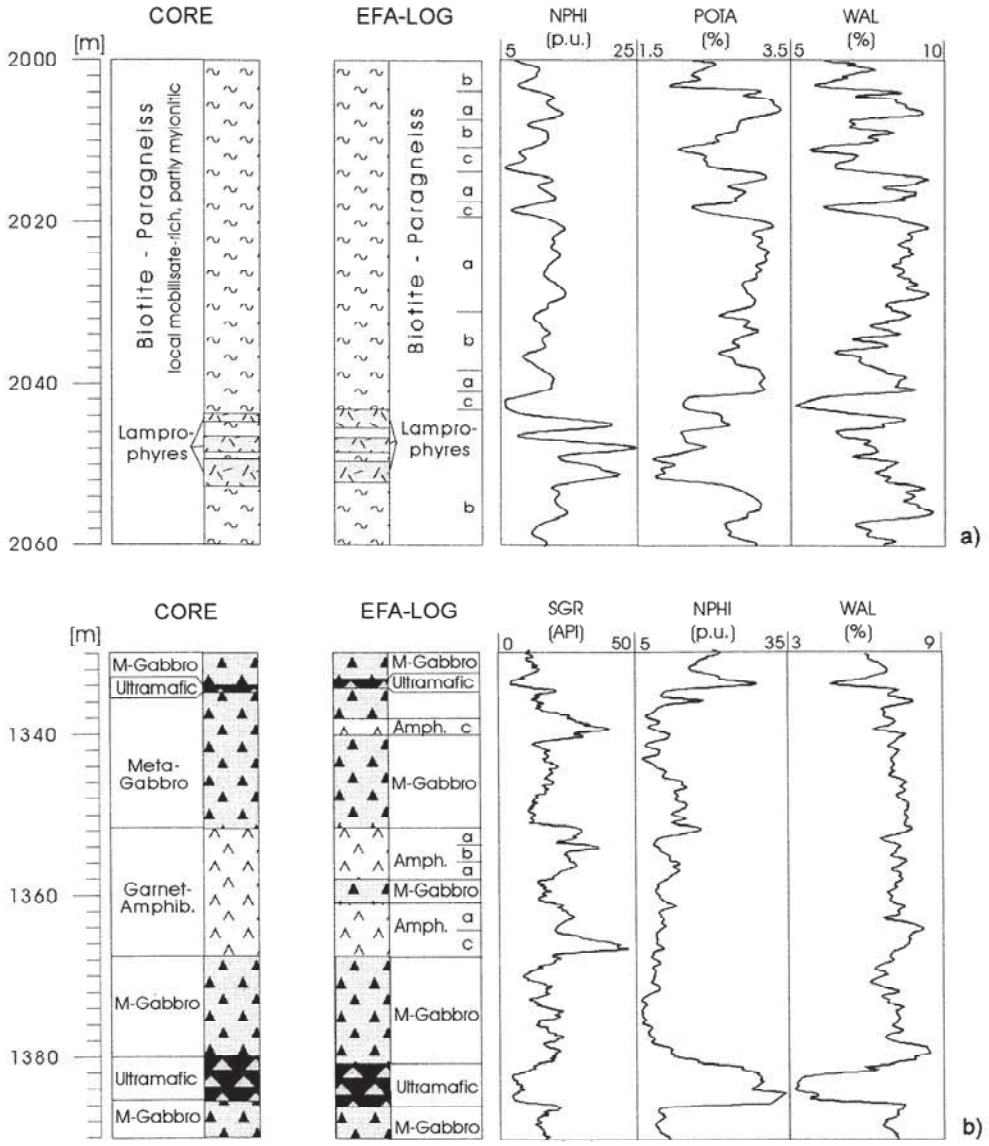

Figure 6. Comparison of the log derived lithology (EFA-log) with the core description of the pilot hole. Shown are depth sections exemplary for (a) the paragneisses with intercalated lamprophyres and (b) the metabasitic units, where amphibolites, metagabbros, and ultramfitites are clearly identified by the logs. The subtypes of the paragneisses (Figure 6a) are defined by the varying quartz-mica content reflected by the logs. From subtypes a to c quartz content is increasing. This is related to lower potassium and aluminium contents, mostly bound in micas. The subtypes of the amphibolites (Figure 6b) are defined by the varying content of quartz-feldspar mobilisates. Mobilization increase from type a to c is reflected by slightly increased γ activity.

crystalline basement rocks. Variations between 10^3 and 10^6 ohm m (LLD) are nearly independent of the main lithology penetrated (Figure 4). Only structural features such as cataclastic overprint produce a notable decrease in electrical conductivity, which is in general related to graphitization and ore mineralization in the shear zones frequently observed in the borehole. In addition, brines in faults and fissures or drilling fluids invaded into disintegrated rock sections might significantly decrease the measured resistivity. These structural effects on the log responses are explained in detail in the second part of this paper.

EFA-Log Compared to Cores of the Pilot Hole

From the relation between log responses and lithology, as described above, all rock types, as well as altered, faulted, and fissured sections penetrated by the pilot well could be distinguished from the logs. As shown in Figure 6, the lithology derived from logs and the lithoprofile from cores are highly correlated. All main rock types distinguished from core descriptions are also marked in the EFA-log. Different subtypes of the amphibolites and gneisses can be further distinguished by means of the logs. Here, the logs respond to small-scale, varying composition within a single rock type, for example, to the quartz-mica variations of paragneisses or to the amount of quartz-feldspar mobilization in the garnet-bearing amphibolites.

Regarding the main rock types, few differences are observed between log and core-derived lithology and these are mostly caused by insufficient depth matching. However, the thicknesses of separated lithotypes differs slightly between the profiles due partly to the larger integration volume of the logging data. Particularly, intercalations of rock types strongly

differing from the surrounding lithology (e.g., aplites which crosscut metabasites) often seem to be thicker in the EFA-log than in the core profile. This is caused by shoulder effects. If intercalations are thin (<50 cm) depth resolution of the logging tools might be insufficient to detect them. Differences might also occur if the petrographical features of rock types are not always consistent with their physical/chemical properties. This is the case in distinguishing metagabbros from garnet-amphibolites. Rocks might be classified by the logs as metagabbros due to their more mafic chemistry, whereas the specific petrographic feature of metagabbro, the relict ophitic fabrics, might not be well pronounced.

Transfer of the Electrofacies to the Main Well

To prevent faulty electrofacies assignments, logs were first checked for systematic differences between the main hole and the pilot hole. This was achieved by means of a statistical comparison of the data obtained from similar lithological sections of the upper 4 km [*Pechnig and Wohlenberg*,1993]. Slight deviations were observed for some of the nuclear measurements of γ spectrometry (NGT) and neutron-activation spectrometry (GST/AACT) and taken into account when transferring the calibrated electrofacies to the logs of the main hole. The physical logs were checked for probable trends with depth, such as systematic changes of density or sonic velocity with increasing pressure. Since no significant gradients were observed, the electrofacies calibrated in the upper part were used for the entire depth section [*Pechnig*, 1996].

Owing to borehole breakouts and the reduced measuring program of the upper and the lower part of the main hole (see Figure 2), the statistical database, constructed under ideal conditions in the pilot hole, had to be modified. Discrimination matrices were calculated to examine the redundant information content of the logs. Thus unmeasured or faulty logging data could be compensated by the most suitable combination of available parameters. Outside the completely measured depth interval between 3000 and 6000 m, in which the transfer of the whole database was valid, some electrofacies had to be combined to form larger groups. Nevertheless, it was possible to distinguish all main rock types, to recognize fault and fissure zones, and to identify lithotypes unknown from the pilot hole, although fewer logs were available [*Pechnig and Wohlenberg*, 1993]. Compared to the cuttings analysis, the high sampling rate of the borehole measurements provides not only better depth resolution, but also better differentiation of the lithological units (Figure 7). This is especially the case within the depth section between 3000 and 6000 m, where all physical and chemical logs are available. Many lithological changes not recognized by investigations on cuttings were identified by means of log interpretation. Examples include the subdivision of metagabbros from amphibolites and the identification of small-scale intercalation of hornblende gneisses or ultramafics

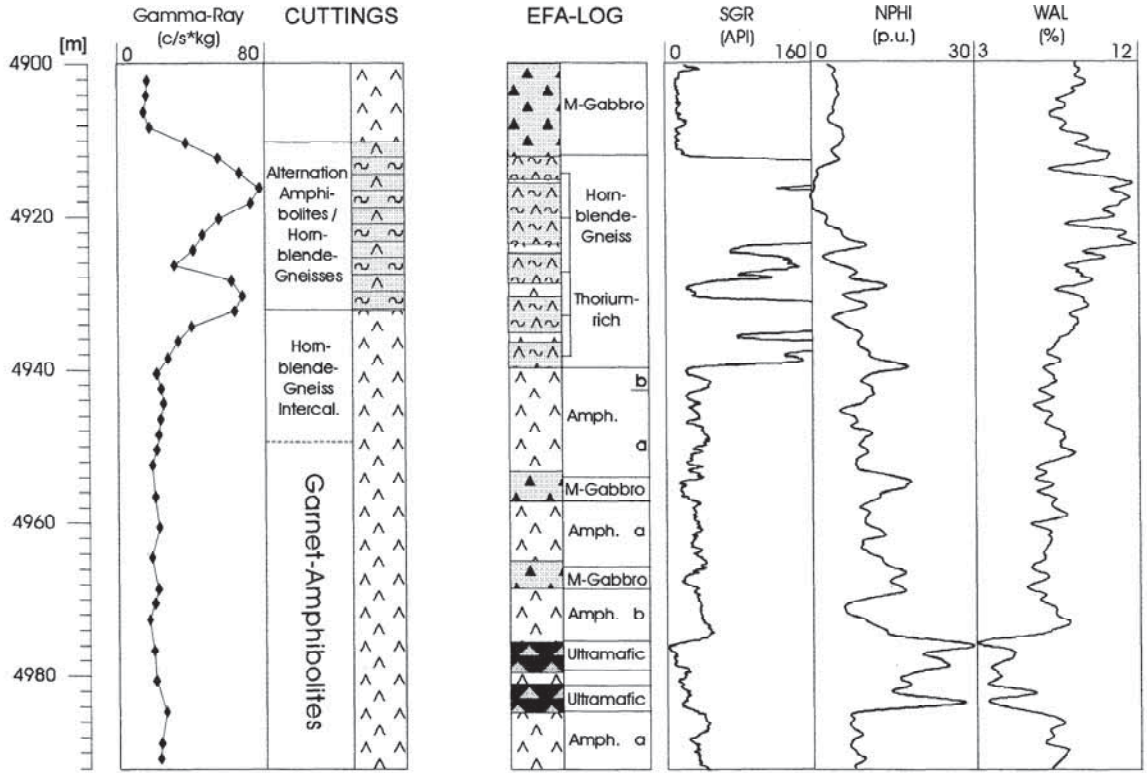

Figure 7. Comparison between the log derived lithology (EFA-log) and the cuttings profile [after *Lich et al.*, 1992] for the depth section 4900-4990 m of the main hole. Logging data provide a much better depth resolution than the cuttings analyses, as can be seen from a comparison of the γ ray measurements. By transferring the electrofacies calibrated in the pilot hole to the main hole, the different types of metabasic rocks were identified. Particularly, the thin ultramafic intercalations are clearly discernible from the neutron porosities and low aluminium values. The thorium-enriched hornblende-gneiss did not occur in the pilot hole and was defined by a new electrofacies.

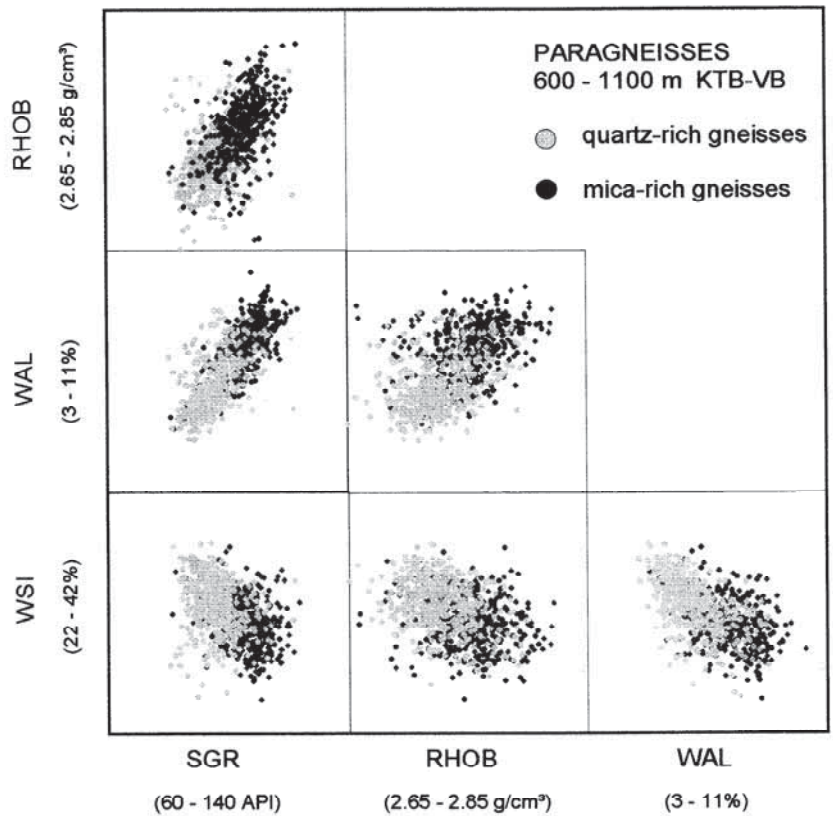

Figure 8. Cross plots between selected logs of a homogeneous paragneiss section transected in the pilot hole. The strong correlations between the parameters are ascribed to the mineralogical composition of the gneisses, within which micas are characterized by higher density, higher aluminium and potassium content (consequently higher γ activity) and lower silicon content than quartz.

within the metabasite section. Such information is very important for petrogenetic and lithostratigraphic questions.

Petrogenetic Information From Logging Data

Although logging data do not give direct information on petrogenetic features, relations can be derived from specific log correlations. Premetamorphic processes such as sedimentation or magmatic differentiation of the protoliths, the metamorphic overprint itself, or retrograde processes of alteration produce variations in composition and petrophysical properties of the main rock types. Such variations were revealed by the logs in all lithological units of the superdeep well.

The paragneisses, for instance, seem to be rather homogeneous with regard to their mineralogical and geochemical composition. However, logging data recorded in these paragneisses clearly reveal certain trends. As displayed in the cross plots of Figure 8, the SGR is positively correlated with rock density and the Al content. This is also valid for the logs POTA, WFE, and NPHI (see Plate 1). All these parameters are negatively correlated with silicon content. These trends are strongly related to the mineralogical composition of the gneisses, which consist mainly of quartz, plagioclase, and phyllosilicates. By taking X ray diffraction data of cores and rock flour into account, it could be demonstrated that intervals showing higher SGR, Al, Fe, and K values correspond to mica-rich layers, whereas zones with higher Si contents correspond to quartz-rich layers in the paragneiss sections. The quartz-rich rock types, with quartz contents up to 60%, have a lower density than the mica-rich gneisses, which have an average quartz content of 35% [*Haverkamp and Wohlenberg*, 1991]. According to diagrams for determination of the sedimentary protoliths [*Wimmenauer*, 1984], the Si-rich gneisses should represent former greywackes, whereas a chemical composition enriched in the elements Al, Fe, and K points to a more pelitic origin. In this case, the log-derived subdivision of the gneisses into quartz-rich and mica-rich layers can be understood as a kind of palaeosedimentological profile, in which the logs reflect the former, alternating sequence of different clastic sediments [*Haverkamp and Wohlenberg*, 1991]. This interpretation was confirmed by additional, detailed, petrographical studies on cores. With respect to the different fabrics of the paragneisses, a twofold division into fine-grained metagreywackes and coarse-grained metapelitic greywackes was ascertained [*Harms et al.*, 1993]. Given the strong correlation between this macroscopic division on cores and the established log derived lithology (Figure 9), it is evident that the physical and chemical log responses provide reliable information to distinguish the protoliths of the gneisses even in the uncored sections of the main hole.

The rocks of the massive metabasic units were distinguished into the main rock types of amphibolites, metagabbros, and the subordinatly occurring ultramafics. Within the amphibolites, the density logs show conspicious small-scale variations in the range 2.7 to 3.1 g/cm³. Data analyses reveal a positive correlation between RHOB and the WSI log, whereas Fe and Ti contents and the NPHI and RHOB are negatively correlated to SGR (Plates 1a, 1c, and 1d). These trends are related to the

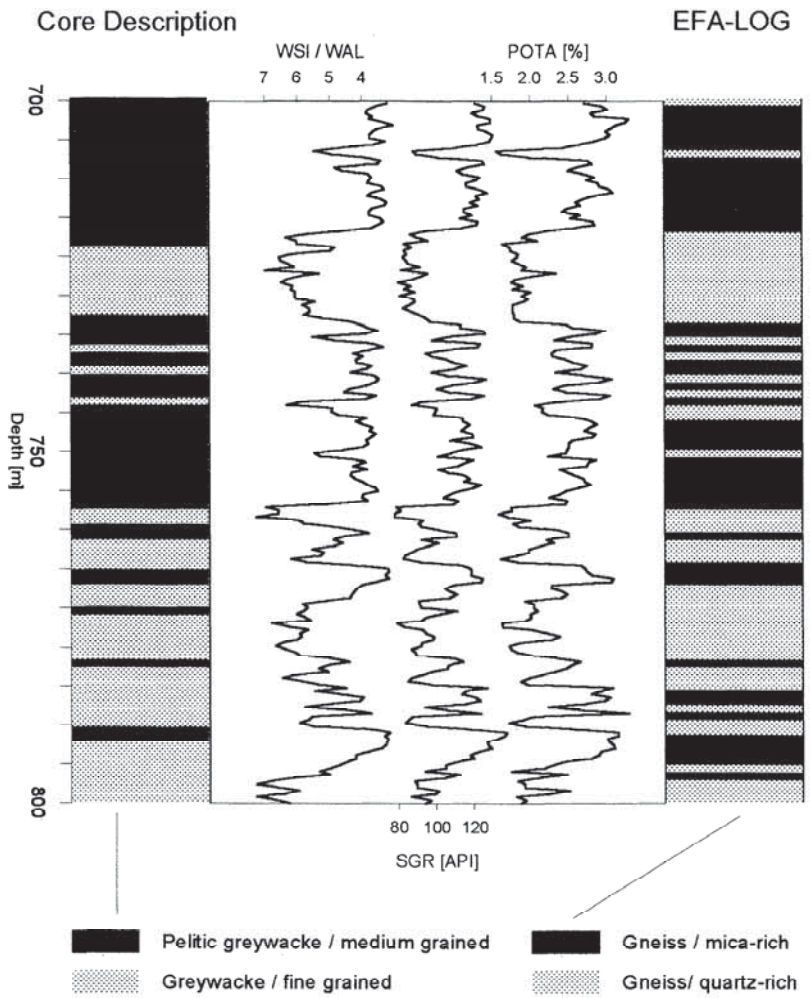

Figure 9. Correlation of the EFA-log with a macroscopic subdivision of paragneisses from core descriptions [*Harms et al.*, 1993], displayed for the depth section 700-800 m of the pilot hole. Mica-rich gneisses subdivided in the EFA-log by higher SGR, POTA, and Si/Al ratio are correlated to rock types, which are defined by their medium- to coarse-grained fabric as metapelitic greywackes. Meanwhile, quartz-rich gneisses correspond to the metagreywackes.

grade of quartz-feldspar mobilization within the amphibolite section. Increased quartz-feldspar contents are clearly correlated with decreasing densities and neutron porosities, lower Fe and Ti values, and strongly increased Si contents. With respect to the varying amount of felsic minerals, three different electrofacies were distinguished in the log derived profile (Figure 6). In this case, the EFA-log helps define the grade of mobilization within the metabasites. Also, premetamorphic differences of the basaltic precursors are partly preserved. For example, chemical logging data reveal significantly different fractionation paths within one large metagabbroic body drilled through between 5600 and 6400 m of the main well. Strong variations of the Fe, Ti, and Al contents in this metagabbro were detected by the logs (Figure 10) and interpreted as the result of early fractionation processes in the magma chamber [*Pechnig and Harms*, 1994].

The varied units are composed of amphibolites, hornblende gneisses, and biotite paragneisses, strongly interfingered on a decameter to meter scale. Compared to the metabasite sections, amphibolites of the varied units are generally characterized by higher γ activity due to their higher K content. This and especially the increased Ti content point to a more alkaline chemical composition (Figure 11), which agrees with the results of whole rock chemical analysis of cores and cuttings [*Harms and Godizart*, 1993].

Lithostratigraphic Correlation Between the Pilot Well and Main Well

The established EFA-logs were finally used for cross-hole correlations between both KTB holes. The main hole is located 200 m southeast of the pilot hole. As displayed in Figure 12, the correspondence between the larger lithological units is obvious. Only by the use of γ activity can a clear correlation between the paragneisses (g units), metabasites (b units) and volcano-sedimentary sequences (v units) be demonstrated. More detailed correlations were established regarding physical and chemical variations within the main rock types.

As displayed in Plates 2a-2c, identical internal sequences were identified in all three lithological units. Comparable successions of alternating quartz- and mica-rich paragneisses are visible for example in the upper paragneiss unit g2 (Plate 2a). In this case, the paragneiss alternations, revealed by the logs on a meter to decameter scale, are grouped for

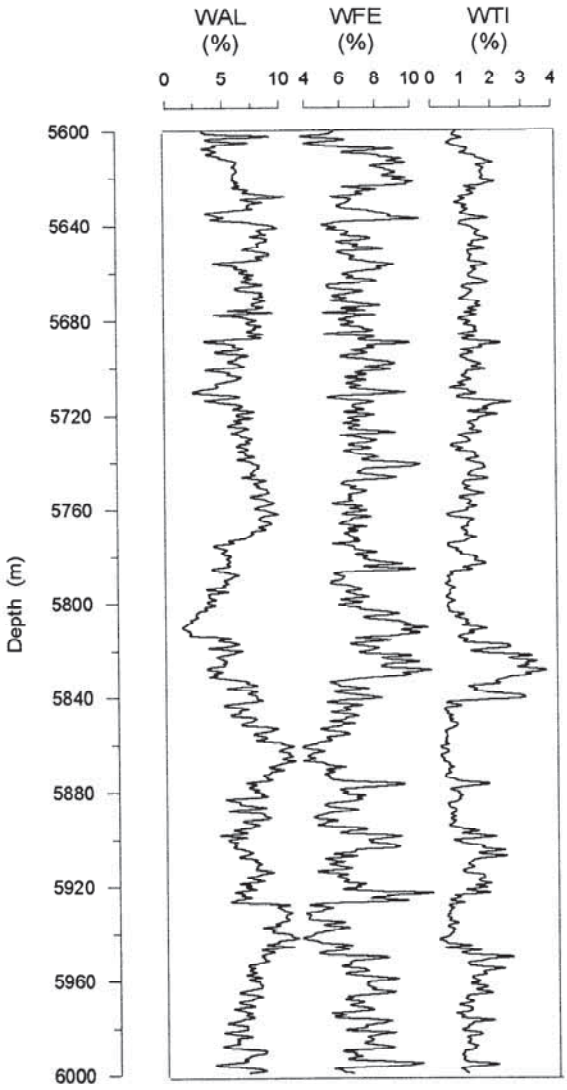

Figure 10. A depth section (5600-6000m) of the main hole where a massive metagabbro body was penetrated. Chemical logs reveal significant variations, which can be related to early magmatic differentiation paths. Whereas higher Al concentrations point to a primitive magma composition, the strong Fe-Ti enrichments indicate a more highly fractionated material. The sharp boundaries of the Fe-Ti-rich layers points to an intrusion of more highly fractionated dikes into the former gabbro of more primitive composition.

comparison to larger units in which mica-rich or quartz-rich types predominantly occur. The volcano-sedimentary units (v2) drilled through in both wells in the depth range between 2400 and 2700 m (Plate 2b) can be divided by logging data into an upper and lower section, separated by an interlayered paragneiss unit. The logs clearly reveal trends within the varied units, reflecting gradual transitions from amphibolitic to gneissic composition. Hence, from logging data, a sedimentary mixing of former volcanic and clastic material can be assumed for the hornblende gneisses of this unit. In the basal part, thin amphibolite intercalations, which are probably derived from former lava flows, can be correlated between the drillholes.

Nearly identical successions also occur in the metabasite unit (b3) below 3500 m (Plate 2c). In this unit, variations are mostly caused by early processes of magmatic differentiation. Corresponding intercalations of ultramafics and more highly fractionated Fe-rich metagabbro occur in both wells. This is also the case for hornblende gneisses (described as augengneisses in the pilot hole), which are possibly products of early mobilization. Further correlations were found for distinctions due to postmetamorphic processes, as is the case for the aplitic dikes at a depth of about 3720 m.

These cross-hole correlations, shown for different lithological units, show that nearly identical successions were penetrated in both wells. Most of the variations in composition, which are similar in large sections of both wells, could be linked to early processes, such as sedimentation or magmatic differentiation. Therefore it can be assumed that the primary differences in composition of the protoliths were widely fixed during the metamorphic overprint of the rocks. This assumption is supported by the chemistry of stable oxygen isotopes. The $d^{18}O$ values indicate preservation of the primary characteristics in the gneisses and the metabasites [*Simon and Hoefs*, 1993].

Estimation of Porosity and Detection of Fracture and Alteration Zones

Estimation of in situ physical properties and investigation of transport processes of fluids in the continental crust are essential objectives of the KTB. Porosity, which cannot be measured directly in situ, plays an important role in controlling these properties. The aim of this work is the realization of a continuous porosity profile of the pilot and the main borehole by the use of logging data. Porosity in crystalline rock is mainly related to cracks and microfractures and to fissures and macroscopic fractures. Porosity due to cracks and microfractures originates during the geological development of the rocks, while fractures and fissures are basically caused by changes of the stress field and temperature. Deterministic and empirical relations between porosity and various physical properties measured by borehole logs, such as density, sonic, neutron porosity, and electrical resistivity [*Serra*, 1984], have been established for sedimentary rocks. By allowing for changes in bulk rock properties due to fluids and gas content it should be possible to use these relations also for porosity prediction in crystalline rocks. However, owing to the small porosities (of the order of a few percent) the results were rather poor. Therefore a statistical approach was utilized. Available data for this work were the borehole measurements and the porosity measurements from cores. To obtain continuous information about porosity, a functional relationship between these data sets has to be found. For this relationship, we assume that porosity is reflected in the available logs. The estimation of porosity is achieved by applying three different but complementary statistical methods. For the first two procedures, the linear regression and the multiple regression, the logs were compared to porosity measurements on cores to establish functional relationships and to determine regression coefficients from which a continuous porosity log is derived. These analyses were carried out in the pilot well, which has been almost completely cored, and then transferred to the main well. In a third approach, factor analysis was applied to the logs. In contrast to the other two statistical methods, factor analysis is independent of calibration and therefore yields only a qualitative result. However, it is generally applicable to well logs without any additional information. In this analysis, the logs were combined to obtain a reduced number of factors representing the essential information inherent in the logs.

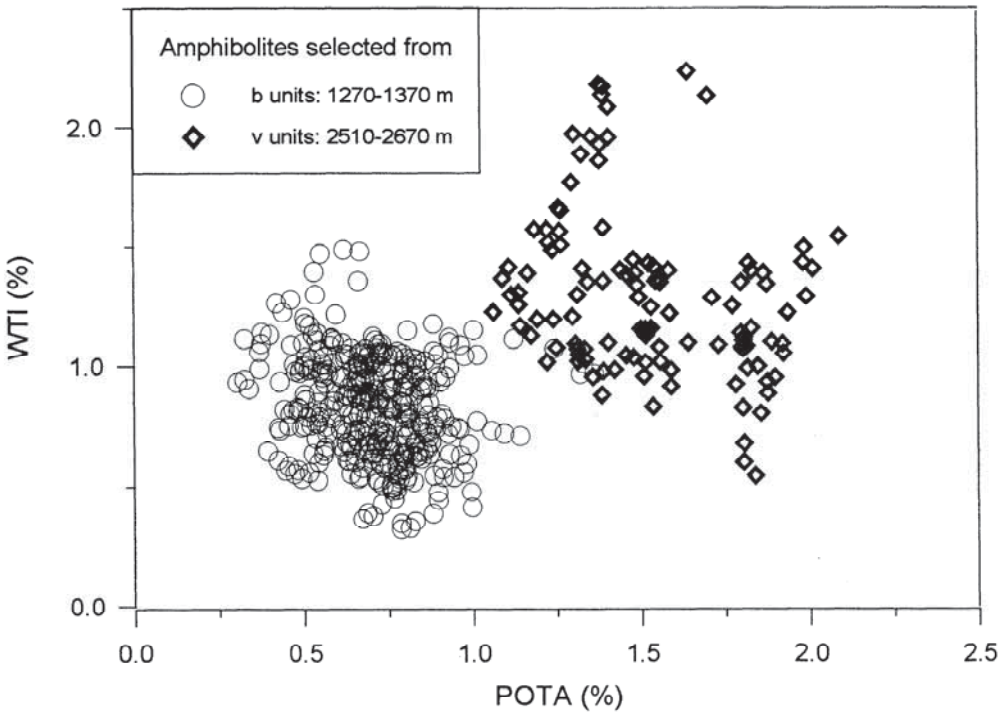

Figure 11. The displayed data are obtained from amphibolites identified by log responses within the massive metabasitic units (b units) and within the volcano-sedimentary units (v units). Amphibolites of the v units are characterized by higher K and Ti concentrations than the amphibolites of the b units, which indicate a more alkaline composition.

Interpretation of potential inflow horizons and cataclastic zones has been performed following all three methods in order to obtain more reliable information than expected from the application of single method.

Before applying the methods of statistical analysis, influences on the borehole measurements due to borehole conditions and lithological changes were corrected (Figure 13). This included the correction of the offset between core depth and logging depth [*Zimmermann et al.*, 1992a] and the elimination of data influenced by severe borehole enlargements. To calculate porosity from borehole measurements by statistical methods, possible influences of rock composition on the logs had to be minimized. Therefore the data sets were separated according to the main lithological units of metabasites and gneisses.

Linear Regression Analysis

Different linear correlations between borehole measurements and core porosity have been carried out on the data from the pilot well [*Zimmermann*, 1991]. Calculation of porosity from the density log failed because the errors in the density log are in the same order as the contrast between the bulk density and the matrix density. Anisotropy prevents the usage of the sonic traveltime, while neutron porosity is mainly due to bound hydrogen in minerals which cannot be sufficiently corrected for. The electrical resistivity of fluid-saturated rocks depends much more on porosity changes. Under the assumption that resistivity is essentially governed by electrolytes within a connected pore space, *Archie* [1950] established an empirical relation known as Archie's law, which has been successfully applied for sedimentary rocks:

$$F = \rho_o / \rho_f = a\ \Phi^{-m}$$

with

F	formation factor;
ρ_o	resistivity of saturated rocks;
ρ_f	resistivity of fluid in the pore space;
m	cementation factor;
a	characteristic constant;
Φ	porosity.

Conversion leads to the following equation used for linear regression:

$$\log \rho_o = \log(a\ \rho_f) - m \log \Phi$$

This equation allows a quantification of the relationship between the resistivities of the laterologs (deep and shallow) and porosity measurements on cores in the pilot well [*Zimmermann et al.*, 1992b]. The porosity of the core samples was measured by the Archimedian buoyancy method under ambient conditions [*Huenges et al.*, 1989]. To limit differences between in situ porosity and measured core porosity due to the effects of pressure at greater depth, calibration was performed only with data from the upper part of the borehole (600 to 1600 m).

First, linear regression analyses were carried out separately for the gneiss and metabasite units. High correlation coefficients (0.65 and 0.80) were obtained for the comparison between measured core porosity and the laterolog devices. For both rock types the calculated regression coefficients (i.e., the slope of regression) are identical within the error tolerances. Hence the varying rock composition of gneisses and metabasites does not influence the resistivity log in a

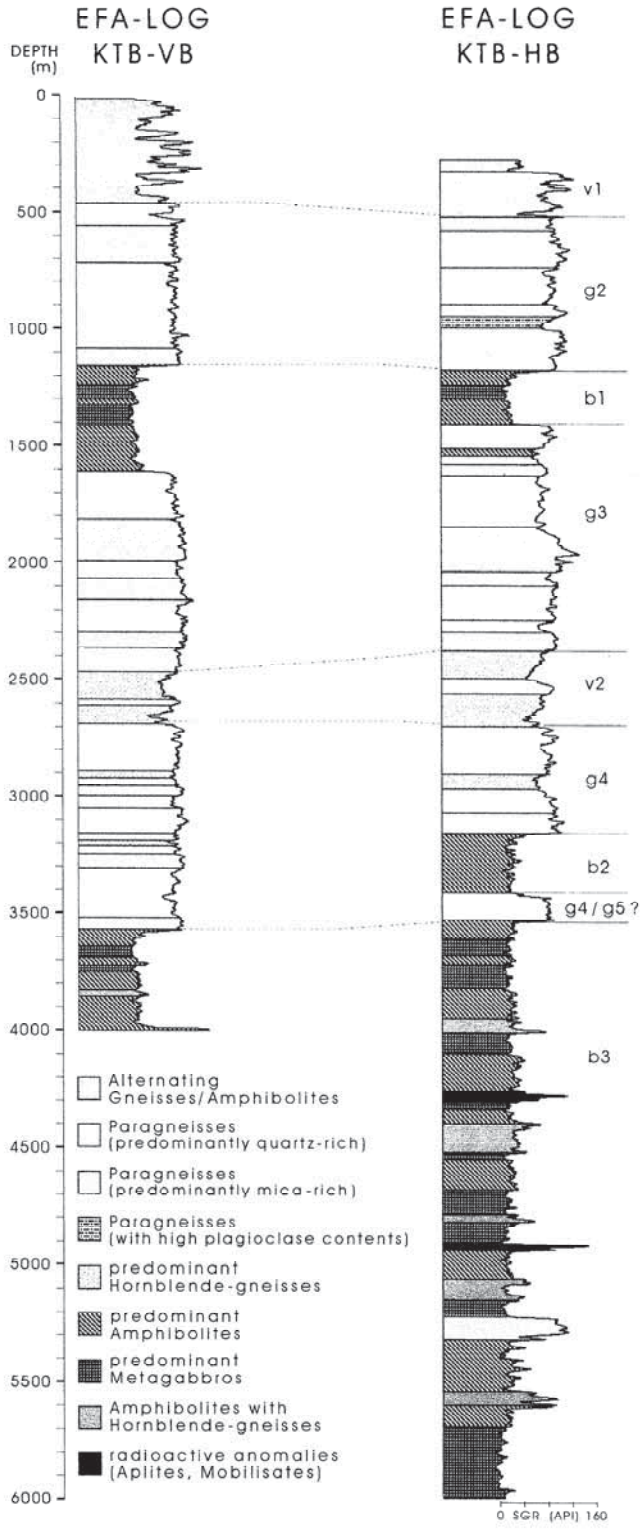

Figure 12. Electrofacies results for the entire pilot hole and the depth section down to 6000 m of the main hole. Clear cross-hole correlations occur for the thick lithological units of paragneisses (g units), metabasites (b units), and volcano-sedimentary sequences (v units).

significantly different way. It is assumed that the matrix of the rock is primarily an insulator for all drilled lithologies. Therefore it seemed appropriate to carry out linear regression using all data. This yielded a correlation coefficient of 0.75 (Figure 14). The calculated regression coefficients (Table 3) are valid for metabasites and gneisses. The significance of regression was tested with a Fisher F test. A significance σ_F of the H_0 hypothesis of $<10^{-4}$ (measure of the error probability) could be obtained. Additionally, the regression coefficients were tested with a T test, according to the Student's T distribution, yielding an error probability s_T of $<10^{-4}$ for the slope m and for the constant a ρ_f in the Archie equation. This indicates a high significance for the regression coefficients.

A continuous porosity log for the pilot hole was obtained by using the regression coefficients to convert the apparent resistivities of the laterolog deep (LLD) into porosity units. As calibration has been performed on cores having porosity values in the range of 0.2% to 4%, only this range in the porosity log should be interpreted as matrix porosity. Values exceeding this range are described in the following as "apparent" porosity because an extrapolation to higher values cannot generally be assumed.

The regression coefficients calculated from the pilot hole can be transferred to any other borehole if the characteristic pore space parameters are similar. This is valid for the main borehole, which has been drilled 200 m from the pilot well into nearly identical lithological successions. Direct calibration of the main hole logs was not possible due to the reduced coring. The interpretation of the calculated porosity log of the main borehole is similar to that of the pilot well. Porosities exceeding the range of the matrix porosity can only be interpreted as apparent porosity, equivalent to a nonscaleable fracture porosity (Figure 14).

Multiple Regression Analysis

The reason for using a multiple regression approach is to increase the statistical significance compared to the linear approach, resulting in a porosity prediction with greater certainty. As with the linear approach, calibration with core data was carried out for the pilot hole between 600 and 1600 m. Using multiple regression analysis, separately performed for the gneisses and metabasites, different log combinations were found to be worth considering for porosity estimation.

Multiple regression analysis in the gneiss section between 600 and 1000 m of the pilot hole results in the following multilinear equation:

$$\Phi = b_0 + b_1 \log \mathrm{MSFL} + b_2\,\mathrm{NPHI} + b_3\,\mathrm{WCA} + b_4\,\mathrm{WFE}$$

The coefficients of regression b_i and the corresponding standard errors Δb_i are listed in Table 4. The significance of the regression coefficients has been tested with a T test to limit the number of coefficients according to significance. Comparing the ratio of b and Δb and the degree of freedom with the T values of the Student's T distribution yields the significance for each coefficient. The degree of freedom is the number of samples (26 for this data set) minus the number of variables involved. The analysis is performed step by step, starting with one variable and increasing the number until a set upper bound is reached. Above that the remaining variance cannot be described by an additional variable without loss of significance. The lower the value of σ_T, the more significant is the result of regression. The upper bound was set in advance to 0.01, equivalent to 1% of error probability. Thus four logs remained in the multilinear equation.

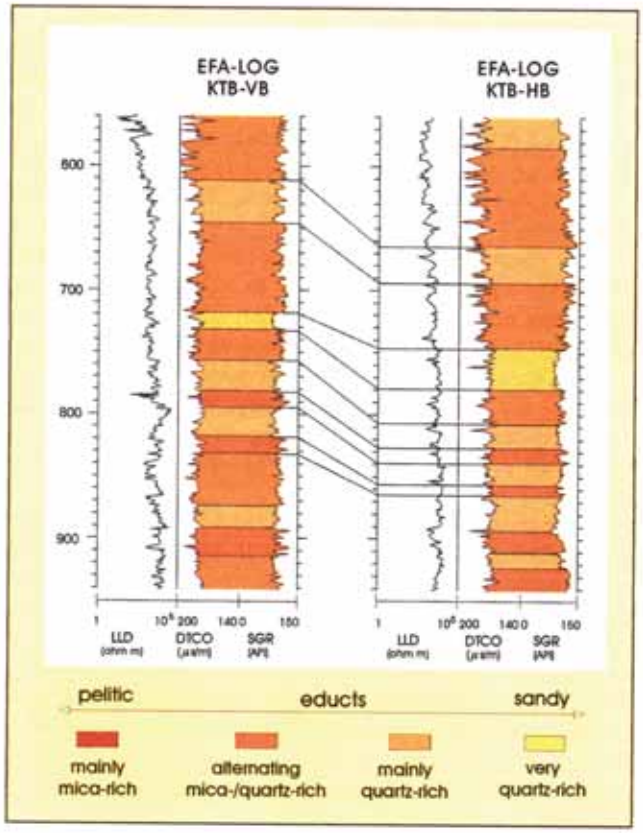

a)

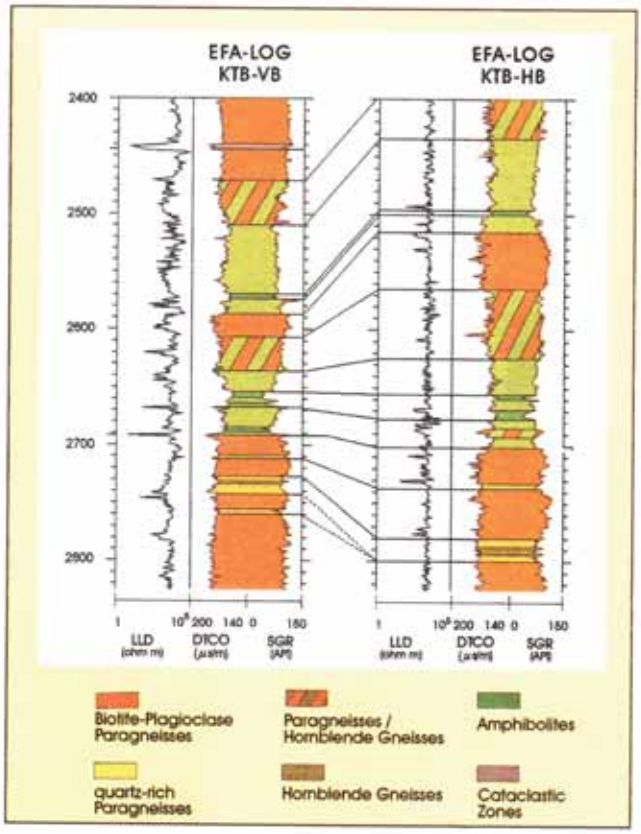

b)

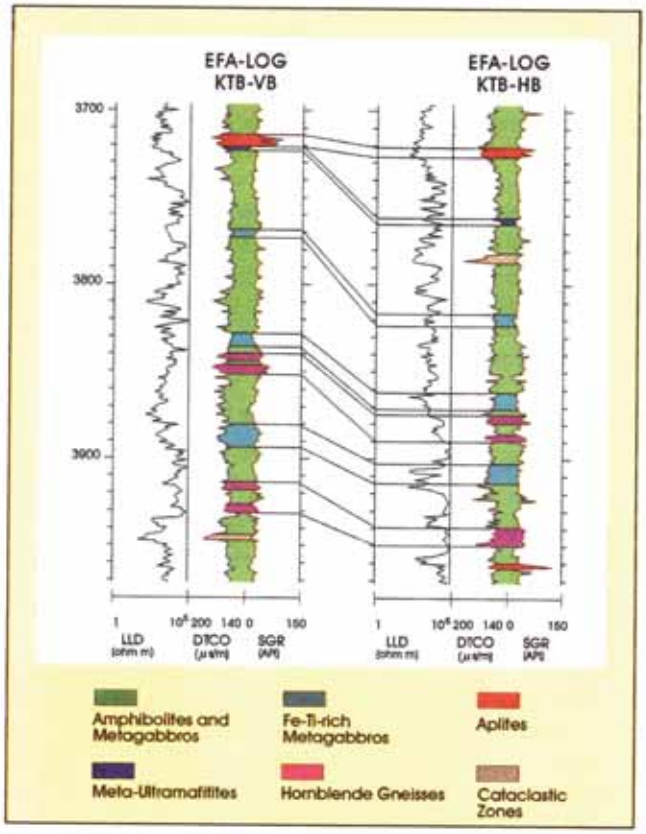

c)

Plate 2. Detailed cross-hole correlations inferred from the EFA-logs of the pilot and main well. Shown are depth sections of (a) the paragneisses, (b) the metabasites, and (c) the volcano-sedimentary units.

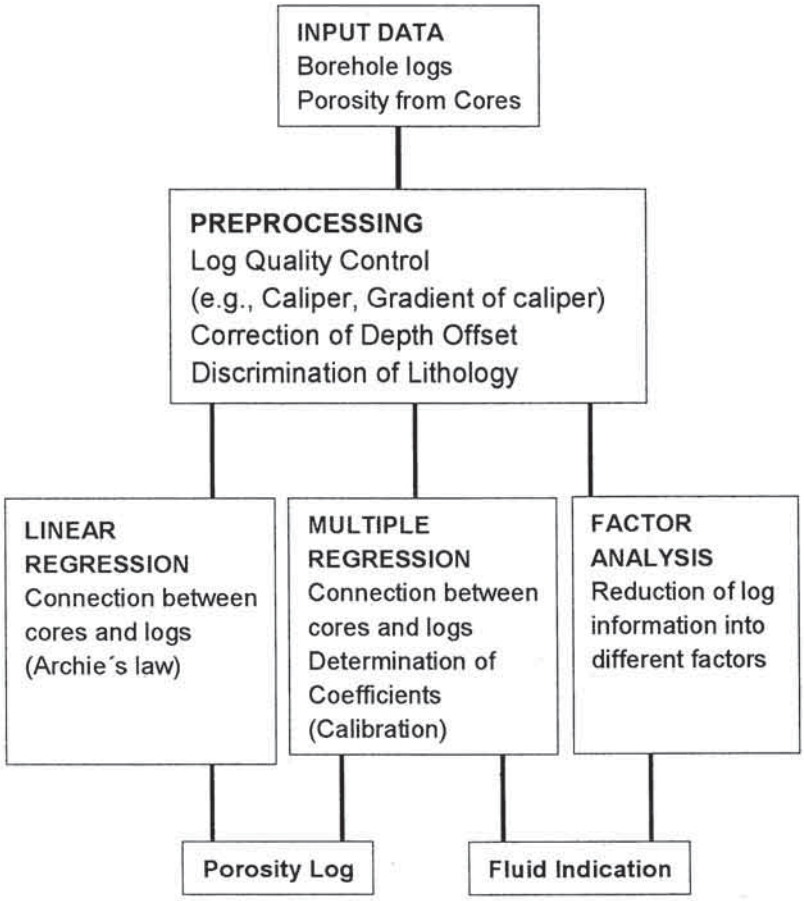

Figure 13. Concept of analysis for porosity estimation.

The main part of the variance is explained by the first two logs (MSFL, NPHI). The microspherically focused log (MSFL) was used instead of the laterolog. This is because, although the correlation coefficient between these logs (0.95) shows their statistical similarity, the focused log explains a higher proportion of the variance. The high degree of correlation indicates that the differing integration volume of these logs has a negligible influence for this data set, implying that the rock is laterally homogeneous. The logs of calcium and iron contents included within the multilinear equation can be interpreted in terms of a correction for lithological inhomogenities. The contributions of these logs to the explained variance are low compared to the contributions of the first two logs in the equation, although the T test indicates that they are still significant.

The calibration for the metabasite section was carried out for the pilot well in the depth range from 1160 m to 1610 m. A statistically significant log combination has been found for this section, analogous to that derived by multiple regression analysis of data from the gneisses. The relation is expressed by

$$\log \Phi = b_0 + b_1 \log \mathrm{LLD} + b_2 \log \mathrm{LLS} + b_3 \log \mathrm{DTST}.$$

The statistical analysis shows a different log combination compared with that for the gneiss section. This results from the statistical approach, which ensures that the analysis includes only those logs which explain most of the remaining variance with regard to high significance of the regression coefficients according to the T test (Table 5).

The multiple correlation coefficients are 0.88 for the gneisses (Figure 15) and 0.81 for the metabasites (Figure 16). Both coefficients are higher than those resulting from linear regression (0.75). Thus, the certainty of porosity prediction could be improved by application of multiple regression rather than a linear approach.

The regression coefficients (Tables 4 and 5) were used to calculate a continuous porosity log down to the final depth of the pilot hole [*Zimmermann et al.*, 1992b]. These coefficients could also be used to achieve a porosity profile for the main well because the lithology is similar to that of the pilot well. However, not all logs used in the equations were measured in the main hole over all depth ranges (Table 2). Down to 3000 m, the logging program was reduced because of the large borehole diameter. Below 6000 m, the use of some tools was restricted by temperature. Therefore the calculation of porosity by the multiple regression approach was limited to the 3000-6000 m depth range of the main well (Figure 17).

Factor Analysis

Factor analysis is a statistical technique used to identify a small number of factors that represent relationships among sets of many interrelated variables [*Cooley and Lohnes*, 1971; *Kendall and Stuart*, 1976; *Backhaus et al.*, 1987]. In this work, the borehole logs (variables) are expressed as a linear combination of factors representing structural and lithological properties of the rocks not directly observable.

In the first stage, factor analyses were carried out on logs

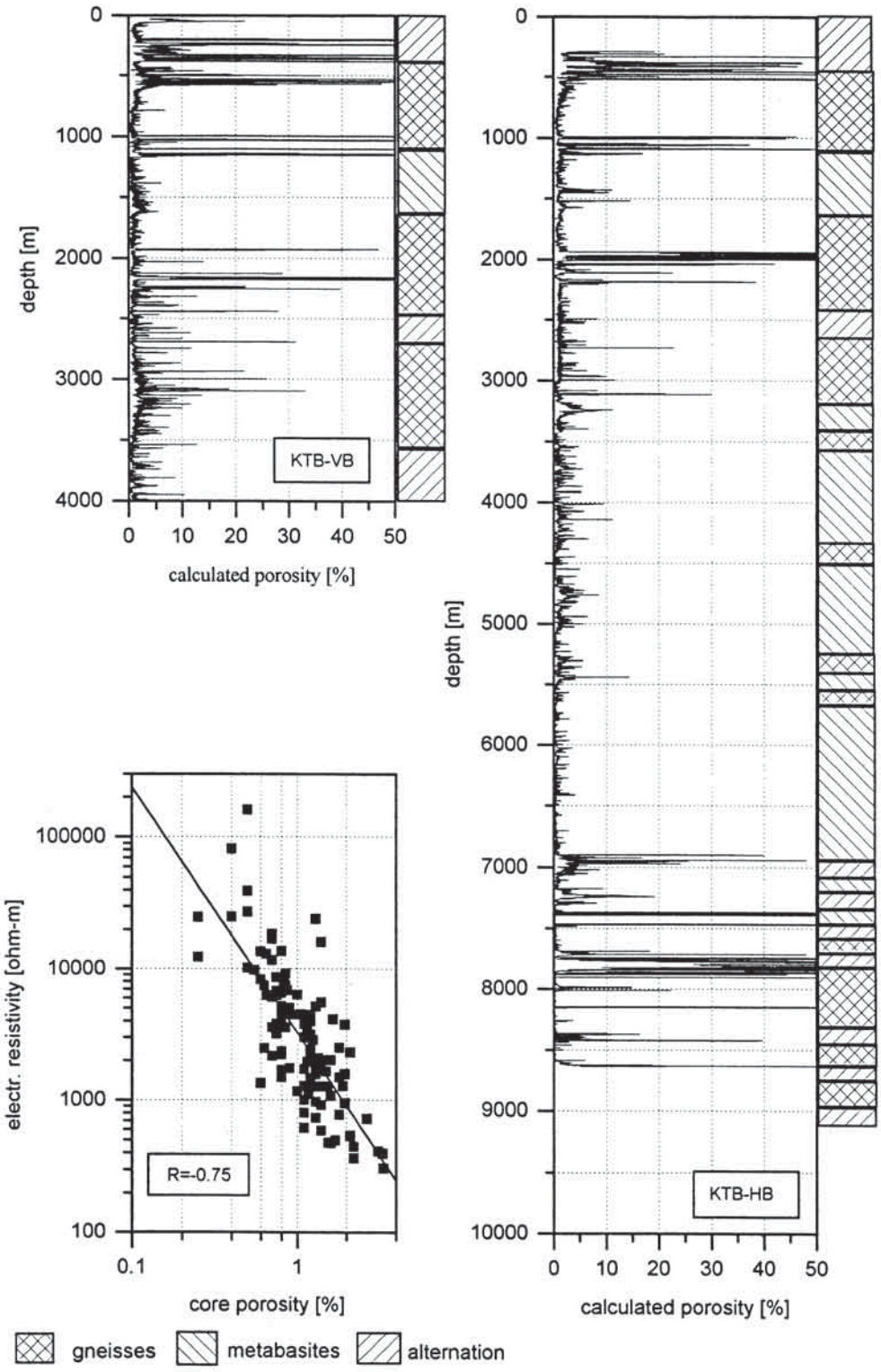

Figure 14. Porosity estimation correlating core porosity and electrical conductivity using a linear approach similar to the Archie equation established for sedimentary rock. The cross plot (lower left) contains the calibration of electrical resistivity from laterolog deep (LLD) with porosity measurements from cores from the pilot well, yielding apparent porosity logs for both boreholes (VB, pilot well, HB, main well). Apparent porosities in the range of the calibration data (<4%) can be interpreted as true matrix porosities, whereas higher porosities are indications of fluid-filled or mineralized fracture zones.

Table 3. Result of Linear Regression Between the Logarithm of the Electrical Resistivity and Porosity According to Archie's Law

Parameter	Value
Number of samples	110
R	0.75
F	142.2
σ_F	$< 10^{-4}$
m	1.86
Δm	0.156
T	11.9
σ_T	$< 10^{-4}$
$a\,\rho_f$	0.622
$\Delta a\,\rho_f$	0.0053
T	107.6
σ_T	$< 10^{-4}$

Data are from the depth range from 600 m to 1600 m of the pilot well of KTB. The cementation factor m and corresponding standard error Δm, the regression constant $a\,\rho_f$ and the corresponding standard error $\Delta a\,\rho_f$, the correlation coefficient R and the significance tests for the correlation coefficient (Fisher *F test*) and the regression coefficients (Student's *T* test) for the converted equation are given.

from the pilot well [*Zimmermann et al.*, 1992b]. These analyses, when performed separately for the gneisses and metabasites, resulted in different combinations of factors. However, in each lithology, one factor was always calculated combining the logs of electrical resistivity and sonic measurements. This factor is highly correlated with the porosity logs calculated by linear and multiple regression. Therefore, this factor could be interpreted as an additional indicator of porosity changes. This was supported by comparison of the factor log with fluid inflow zones indicated in the pilot hole by temperature logging. It seems appropriate to establish a similar log from factor analysis for the main hole, which can be interpreted in the same way as for the pilot hole.

Factor analyses were carried out in the main hole separately for gneisses and metabasites in the depth range from 3000-6000 m. Limitation to this depth range is due to the reduced logging program conducted in the other depth ranges (Figure 2). The analyzed depth section was subdivided at 4500 m for two different runs of the logging program. The number of factors was determined following the so-called "Kaiser criterion" [*Backhaus et al.*, 1987], taking into account only factors with eigenvalues exceeding 1. In the main hole, five (depth section 3000-4500 m) and six factors (depth section 4500-6000 m) represent between 65% and 80% of the whole variance. These

Table 4. Regression Coefficients b_i With Corresponding Standard Errors Δb_i and the Results of the Significance Test (Student's *T* test) of the Regression Coefficients for the Paragneiss Section from 620 m to 1000 m of the Pilot Well

Variables	b	Δ b	T	σ_T
MSFL	-0.356	0.0662	-5.383	0.0000
WCA	-0.090	0.0210	-4.394	0.0003
NPHI	0.111	0.0260	4.248	0.0004
WFE	-0.185	0.0540	-3.415	0.0026
Const.	2.157	0.3110	6.937	0.0000

Table 5. Regression Coefficients b_i with Corresponding Standard Errors Δb_i and the Results of the Significance Test (Student's *T* Test) of the Regression Coefficients for the Amphibolite Section from 1228 m to 1610 m of the Pilot Well

Variables	b	Δ b	T	σ_T
LLD	-0.914	0.219	-4.174	0.0002
LLS	0.629	0.204	3.080	0.0037
STDT	7.327	2.580	2.840	0.0070
Const.	-19.668	7.310	-2.691	0.0103

factors were transformed by "varimax-rotation" [*Backhaus et al.*, 1987] to get a more simple structure. Table 6 shows all factors and the corresponding factor loadings (statistical term for individual weights of the logs) calculated for the main well. The factors can be interpreted according to the weight of the respective loadings. The values of the factor loadings vary between -1 and +1. Values close to zero do not contain any information. A higher absolute value of the loading implies that the influence of a specific variable is greater and should therefore be better characterized. For interpretation of the factors, only loadings are chosen exceeding a given threshold (here +/- 0.5).

Factor analyses in the main hole resulted in factors with properties similar to those in the pilot well. Most of the factors identified are related to rock composition, i.e., mineralogical and geochemical variations (columns 2-6 of Table 6). For example, changes in the quartz content of the rocks are expressed in terms of a strong anticorrelation between the silicon and calcium logs. These two logs are combined into the single factor displayed in column 2 of Table 6. Changing rock densities, caused by the varying mineralogical composition, are reflected by the factor primarily combining the logs of the Litho

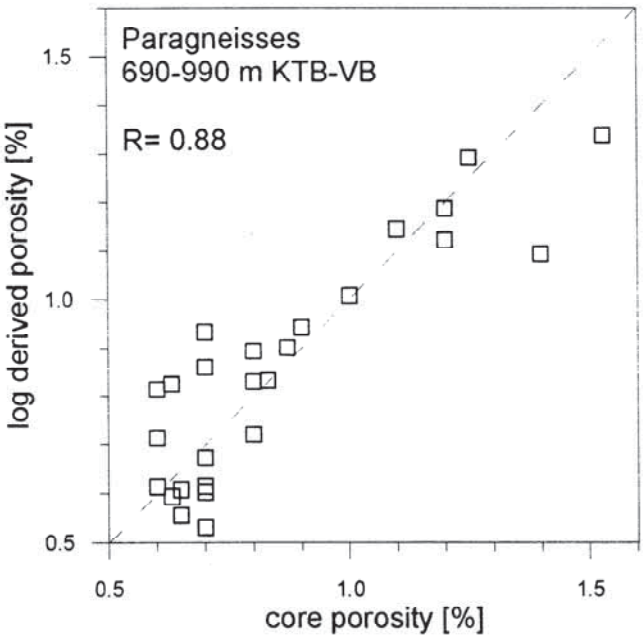

Figure 15. Correlation between measured porosity and calculated porosity from multiple regression in the gneiss section of the pilot hole [*Zimmermann et al.*, 1992b].

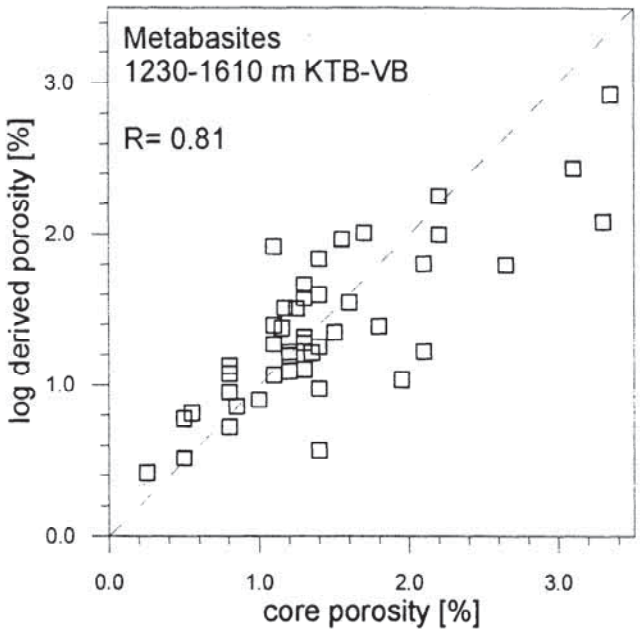

Figure 16. Correlation between measured porosity and calculated porosity from multiple regression in the amphibolite section of the pilot hole [*Zimmermann et al.*, 1992b].

Density Tool (column 3). Changes in radioactivity are not only controlled by the whole rock composition but also by the occurrence of radioactive accessories. For example, thorium and uranium-rich accessories are frequently observed in the metabasite sections and caused by secondary processes such as hydrothermal activity (column 4). The factors in column 5 are related to chemical differences. These might be caused by differences of magma fractionation within the metabasites and intercalations of basic rocks within the gneiss sections.

Besides the factors related to rock composition, one factor characterized mainly by a combination of resistivity and sonic logs was calculated for all subsections. The neutron porosity log is included subordinately. This factor, displayed in the column 1 of Table 6, can be interpreted as for the pilot well as a fluid and fracture indicator. The factor log calculated for the main hole between 3000 and 6000 m is shown in Figure 17 (right column). The log obtained is plotted on a standard scale, i.e., with zero means and unit variance for the specific dataset. Positive factor values, related to high sonic travel times and low resistivities, indicate zones of increased porosities, i.e., alteration and fracture zones.

Log Responses Related to Cataclastic Overprint and Alteration

Statistical analysis leads to different porosity profiles containing varying information according to the logs involved. In order to understand the causes of porosity increases, we compared the calculated porosity logs with lithological and structural information.

Different stages of ductile and brittle deformation resulted in abundant numbers of faults and fractures [*Zulauf*, 1991]. The ductile shear zones do not produce remarkable contrasts in the physical and chemical log responses, as is the normal case in cataclastic overprinted and fractured depth sections. The observed types of cataclastic overprint and alteration, which are often closely related, were, however, reflected by the logs in different ways. A very sensitive parameter to cataclastic overprint is the electrical resistivity. This is because sulfide ore mineralization and strong graphitization on brittle shear zones in paragneiss sections create significant increases in electrical conductivity. Whereas undisturbed paragneisses are characterized by resistivities of 100,000 ohm m or more, even thin, interconnected, graphite films will reduce the observed resistivity down to values of less than 100 ohm m. Such sharply decreased resistivity is not only due to the above mentioned electronic effects but to fracture porosity caused by electrolytes in a saturated pore space. This effect is locally limited to the range of decimeters. Therefore the interpretation of the result of the linear regression is ambiguous: The increase in the porosity log may be due to the increase of matrix pore space and fractures filled with electrolyte or may be produced by the rather high electronic conductivity of ore minerals and graphite. In the case of graphite-bearing fractures, the linear porosity log shows distinct peaks, reaching unrealistically high values of more than 50%. This can frequently be observed in the pilot hole and the main hole, i.e., within important fracture zones around 1000 m and 2000 m, and between 7000 to 8000 m (Figure 14). Porosity predicted by multiple regression is not as strong effected by ore and graphite contents. For example, a limited, graphite-bearing, fracture zone was transected in the main hole around 3100 m, producing a peak of up to 30% "apparent" porosity in the linear calculated log (Figure 14). In contrast, the porosity log from multiple regression shows realistic values, only ranging between 2 and 3% (Figure 17).

Owing to the degree of mechanical disintegration of the rocks, cataclastic zones are further characterized by reduced seismic velocities and increased neutron porosity values. These parameters are most important for the identification of faults and fissures within the metabasite units. Since shear zones occurring in metabasites are normally free of graphite, strong resistivity contrasts like those in the paragneiss sections were not observed. In this case, the measured resistivity is mainly influenced by circulating fluids or penetration of drilling fluid into open faults and fissures. Therefore porosity calculations based on the linear approach are more reliable in the metabasites than in the paragneisses. The predicted values are normally less than 5% (Figure 14) and match better with the range of porosity values estimated from multiple regression analysis (Figure 17).

Retrograde, overprinted, depth sections mostly correspond with zones of increased rock porosity. This is especially the case in altered, strongly epidotized metabasites. In contrast to the porosity bound to discrete zones, as described above, the effect on the structure sensitive logs RHOB, LLD, NPHI, and DTCO is less pronounced. Increased porosity in such zones affects log responses more gradually (e.g., 3200-3400 m of the main well, Figure 18) and does not produce strong peaks as faults or fissures do. This observation points to a real matrix porosity, increased within this section and related to the grade of alteration. Such an increased porosity can be explained by the process of epidotization, which takes place under the influence of circulating fluids. Since the replacement of plagioclase by epidote is connected to a negative volume balance, porosity and permeability will simultaneously increase [*Möller*, 1986].

Comparison of the Results in Hydraulically Active Depth Ranges

Hydraulically active zones identified by active and stimulated fluid inflows were frequently observed within the

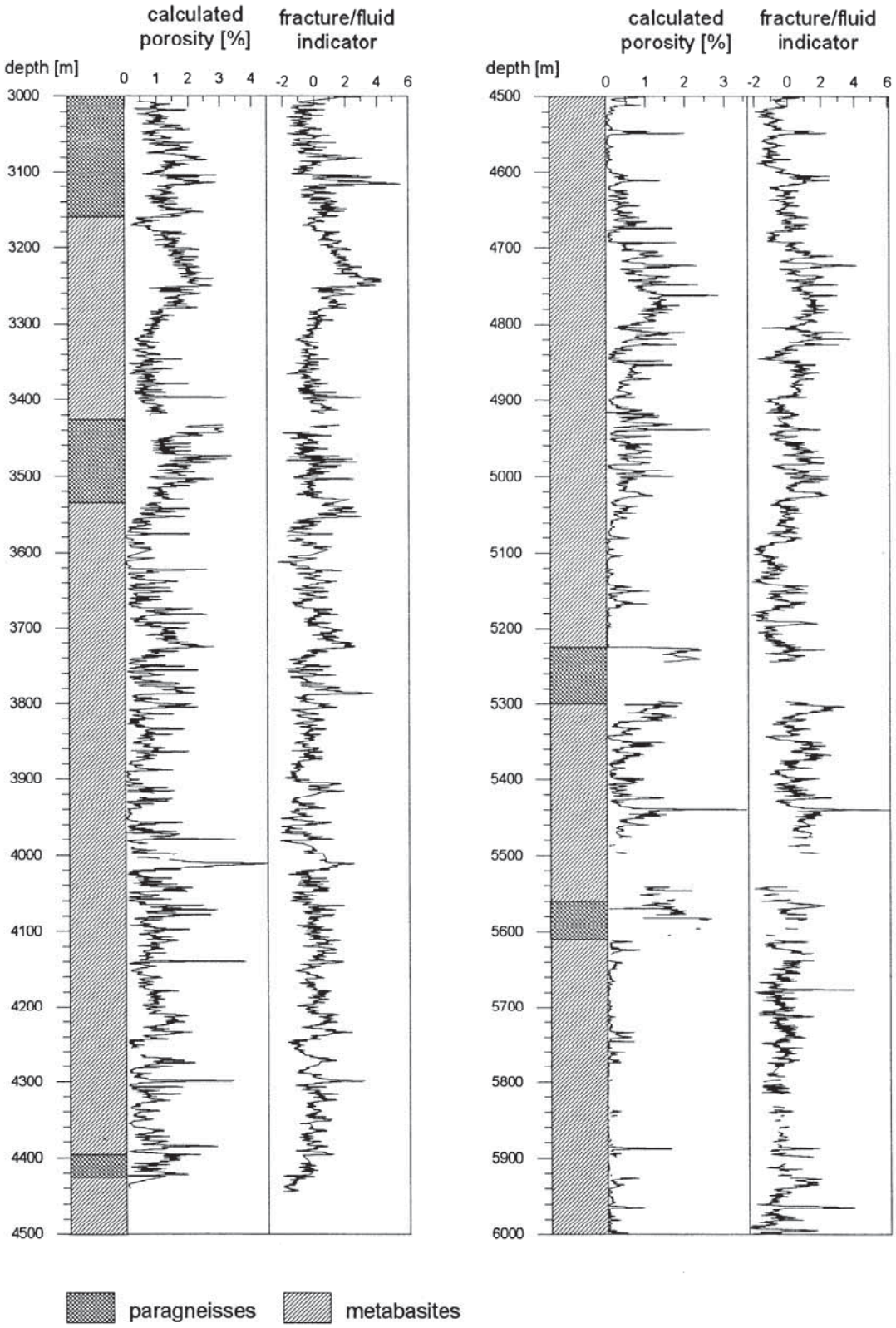

Figure 17. Porosity log from (left) multiple regression and (right) factor log from factor analysis for the depth interval 3000-6000 m in the main hole. Results from factor analysis correspond well with those of the pilot well [*Zimmermann et al.*, 1992b]; the factor log is interpreted as a fluid/fracture indication log. Lithology indicators come from the geological investigations on cuttings and log data [*Duyster et al.*, 1995; *Pechnig*, 1996]. Depth ranges without porosity estimation are due to caliper influences (exceeding of caliper threshold).

Table 6. Factors Calculated for the Depth Section 3000-6000 m of the Main Well and Their Corresponding Logs

Metabasite Sections Between 3000 m and 4500 m					
Fracture, Fluid Related Factor	Factors Related to Mineralogical and Chemical Variations				
24.0 %	6.5 %	12.8 %	6.2 %	21.1 %	
DTCO +0.76 DTSM +0.84 DTST +0.62 LLD - 0.90 LLS –0.89 NPHI +0.61	WCA+0.93 WSI -0.92	PEF –0.50 POTA +0.65 RHOB –0.64 WAL +0.65	THOR +0.71 URAN +0.80	WFE +0.86 WGD +0.89 WTI +0.87	
Metabasite Sections Between 4500 m and 6000 m					
Fracture, Fluid Related Factor	Factors Related to Mineralogical and Chemical Variations				
19.4 %	7.5 %	17.4 %	10.8 %	11.6 %	7.0 %
DTCO +0.67 DTSM +0.80 LLD –0.87 LLS –0.73	WCA +0.88 WSI -0.92	PEF +0.94 RHOB +0.72 U +0.98	THOR +0.76 URAN +0.70	WFE +0.85 WGD +0.84 WTI +0.83	NPHI –0.58 WAL +0.89
Paragneiss Sections Between 3000 m and 4500 m					
Fracture, Fluid Related Factor	Factors Related to Mineralogical and Chemical Variations				
25.0 %	13.4 %	10.7 %	9.5 %	6.8 %	
DTSM +0.67 NPHI +0.69 LLD –0.85 LLS –0.82	WCA –0.92 WSI +0.86	PEF +0.75 POTA +0.62 RHOB +0.70	DTCO +0.73 THOR –0.62 WAL +0.68	WFE +0.62 WGD +0.82	
Paragneiss Sections Between 4500 m and 6000 m					
Fracture, Fluid Related Factor	Factors Related to Mineralogical and Chemical Variations				
9.0 %	10.9 %	11.8 %	15.9 %	25.6 %	6.8 %
DTCO +0.51 DTSM +0.77 LLD -0.76 LLS -0.62	WCA -0.92 WSI +0.85	PEF +0.87 U +0.98 RHOB +0.59	THOR +0.81 WAL +0.85 NPHI -0.67	WFE +0.92 WGD +0.74 WTI +0.79 POTA -0.57	URAN –0.86

Only logs with factor loadings exceeding the threshold of 0.5 are displayed. Plus and minus signs relate to the correlation between the logs and the factor. The percentages give the contribution of the specific factors to the whole variance of the data sets.

pilot hole and the main hole [*Kessels and Kück*, 1995; *Huenges et al.*, this issue]. Highly saline inflows were stimulated in several zones by hydraulic drawdown tests in which removal of the drill string causes a drop in the mud level. A measure of the salinity of a fluid inflow is a decrease of the electrical mud resistivity. Figure 18 shows the reduced mud resistivity log (linear trends are subtracted) in the depth section between 3000 m and 6000 m of the main hole. Four depth sections, characterized by a considerable decrease of the mud resistivity log, can be clearly identified as fluid inflow zones. The lower boundaries of these zones can be taken as the intrinsic inflow position, taking into account a lower density of the invading fluid compared to the mud. Fluid inflow into the borehole above this lower boundary is also possible but is not necessarily marked by an additional decrease in mud resistivity, because the inflow may invade over a wide area and may even overlap. Therefore a clear depth location of single fluid inflows is difficult.

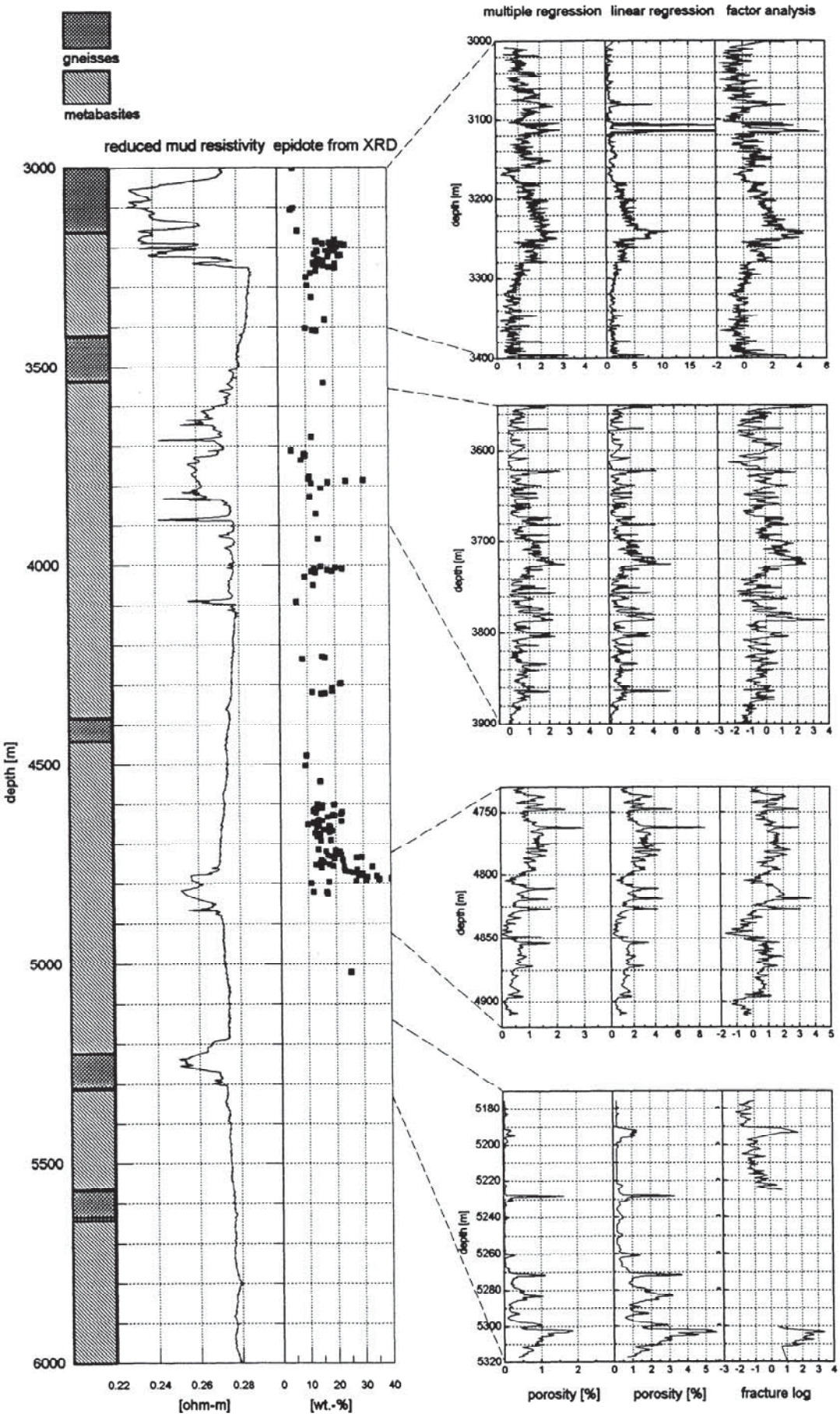

Figure 18. Comparison of the calculated porosity logs and the factor log with the reduced mud resistivity log of the drawdown test from March 23, 1992. Displayed are data in the depth range from 3000 m to 6000 m. Epidote data are from X ray diffraction analysis. Saline inflow is characterized by decrease of reduced mud resistivity, where "reduced" means the subtraction of the linear trend. Displayed on the right are four subsections with fracture zones indicated by a higher 'apparent' porosity. The decrease in mud resistivity implies the existence of high-salinity inflow. In the lowest subsection, the gap in the factor log is due to enlargement of the borehole.

A comparison of the reduced mud resistivity log and the porosity and factor logs, calculated by statistical analyses, was conducted in detail for such hydraulically active zones (Figure 18). The following discussion considers the extent to which the calculated porosity logs can be used for an identification and characterization of fluid inflow horizons.

The first subsection in Figure 18 is characterized by a decrease of the reduced mud resistivity in the depth range from 3050 m to 3250 m due to an inflow during the drawdown test. The inflow position is most probably located at the sharp lower boundary at 3250 m. This correlates with higher values in the porosity and factor logs in this depth range. These increases in porosity are characterized in the logs not by the single, locally limited peaks to be expected at distinct fractures but by increases of a few percent over a wide area of approximately 100 m. This indicates a larger area of increased matrix porosity. A probable reason for this increased matrix porosity is the increased content of epidote, a mineral occurring in the surrounding of fault zones and indicative of strong alteration. The epidote profile from X ray diffraction analysis shows an increase of epidote up to 20% in this depth range. However, the inflow at about 3250 m does not seem to be the only one in this subsection, since above this depth range the reduced mud resistivity shows additional minima. The porosity and factor logs in the depth range of about 3100 m show several peaks, which can be ascribed to increased fracture porosity. The unrealistic, high, values calculated from linear regression indicate the occurence of graphite in these fractures.

The other subsections in Figure 18 are also characterized by various inflow horizons, each spanning an area of about 100 m. From the mud resistivity alone is not clear where the real inflow should be assumed or to what cause the origin of the permeability should be ascribed to. If epidotization were present, matrix porosity would be one potential origin of the inflow, whilst any open faults which may be present should not be neglected. The epidote content increases at the depth intervals of 3800 m and 4800 m, indicating higher matrix porosity, which can also be supported by the porosity and factor logs. The decrease of resistivity in this metabasites is mainly an electrolytic effect (see previous section), visible by the similiar shapes of the porosity logs calculated from linear and multiple regression. The mud resistivity decrease below 5230 m is related to gneisses which are usually free of epidote. The distinct porosity increases derived from the logs here are probably due to single fractures where inflows are possible. Decreases of electrical resistivity in fractured paragneisses are often caused not only by fluid salinity but also by graphitization, as is the case at 3100 m depth. However, this effect seems not to be so important in this depth sections (5200-5300 m) indicated by the rather small porosity values derived from the linear approach. The lowest boundary of decreased mud resistivity is located at 5300 m, probably indicating the bottom of the inflow horizon. This corresponds with the highest values in the porosity logs derived from the linear and the multilinear approaches. At 5270 m, the mud resistivity decreases over a depth range of 15 m, with the lowest resistivity at 5255 m. This corresponds with the peaks in the porosity logs which could be additional inflow zones.

Conclusion

Integrated interpretation of logging data recorded in the KTB scientific wells provide significant insights into the composition, structure, and physical properties of the continental, crystalline crust. Comparative studies of downhole log responses, petrographical examinations, and geochemical and petrophysical laboratory data allow a reliable calibration of downhole measurements with lithological and petrophysical features of crystalline basement rocks.

Based on the electrofacies concept, synthetic borehole profiles, called EFA-logs, were established. These EFA-logs represent a continuous and detailed reconstruction of the drilled lithology of the KTB pilot and main holes. The log-derived lithological profiles provide information for distinguishing between different rock types, identifying alteration and cataclastic overprints, and recognizing petrogenetic features. It could be demonstrated that in crystalline rock electrofacies, once calibrated, can be transferred from one well to another where similar lithologies can be assumed. Hence it was possible to apply electrofacies data from the pilot hole to the main hole, where the available logging data set was partly limited, due to enlarged bit size (in the upper part) and limitations of the logging tools resulting from breakouts and temperature increases (in the lower part). In uncored sections, the high sampling rate of borehole measurements provides not only better depth resolution than analysis of cuttings, but also better differentiation of the lithological units.

The EFA-logs established in the pilot hole and the main hole were used for lithostratigraphical comparison between the two wells. In addition to the main lithological units and extended fault zones, which are significantly identical in both wells, correlations between both wells also exist for internal variations within the main lithological units. Such variations could be related to premetamorphic processes such as sedimentation of the gneissic protoliths and early magmatic differentiation of the metabasites. Identical successions of former sandy and pelitic material within the paragneisses could be correlated between the boreholes, as could early intercalations of ultramafitites and more highly fractionated metagabbros within the metabasite sequences. This indicates the existence of very similar rock sequences in both wells, in which the primary differences in composition were largely fixed during metamorphism and deformation.

A relationship similar to Archie's law, established for sedimentary rocks, between porosity and electrical resistivity allows the calculation of continuous porosity logs for the pilot well and the main well. These porosity logs cannot generally be relied on to provide absolute rock porosities, since electrical resistivity may be controlled by petrophysical and lithological properties such as graphitization and ore mineralization. This leads to an overestimation of porosity, particularly at faults and fractures within the paragneiss sections. Additional information from the logs obtained through multiple regression and factor analysis offers the possibility to separate the different mechanisms responsible for decreased resistivity, the influence of graphitization and mineralization on these approaches being lower than for the linear regression. Multiple regression combines several logs influenced by porosity to calculate more reliable porosity logs than is achievable by the linear approach. Factor analysis relates the information inherent in the logs to factors representing different rock characteristics, and leads to a qualitative parameter which can also be used to indicate fractures and zones of elevated fluid content. These porosity and factor logs were compared to the mud resistivity measurements carried out during a drawdown test and were found to be useful for identifying and characterizing active inflow horizons.

The analyses show that zones of increased porosity occur down to the final depth of the KTB hole. Reliable information on absolute porosity values is only given for the depth section down to 6000 m, where multiple regression analyses could be carried out. The calculated porosity values in this depth range are generally smaller than 5%, even in hydraulically active zones. Comparison of the porosity logs with the lithological information obtained from the EFA-log and cutting analysis shows that increased porosity and related permeability can be ascribed to two different causes: discrete planar discontinuities, such as distinct faults and fractures, and zones of high alteration extending for 10 m or more. Increased matrix porosities occurring in the alteration zones could be related to strong epidotization of the rocks. This form of alteration is possibly produced by a retrograde process of fluid motion, with simultaneous replacement of plagioclase by epidote. Since this replacement is connected with a negative volume balance, this process could gradually produce an increase in matrix porosity. The results show that in addition to fluid inflow through distinct fault zones and other cataclastic zones, there also exist extensive alteration areas of slightly increased matrix porosity, which correspond with hydraulically active inflow horizons.

Acknowledgments. We would like to thank the KTB logging group in Hannover and Windischeschenbach for providing us with the borehole-geophysical data and to the colleagues of the former KTB Field Laboratory in Windischeschenbach performing all the measurements essential for the calibration of the logs. Considerable improvements to the manuscript were made from useful commentary and critical review contributed by P. Nelson, P. Harvey, and V. Haak. Many thanks also to A. Bartetzko for her constructive input on statistics and to F. Simpson for her corrections on grammar and style. We are grateful to Western Atlas International, Inc. for supporting us with log interpretation software, which is most helpful in handling the logging data and we would like to thank the Bundesministerium für Bildung, Wissenschaft und Forschung (BMBF) and the Deutsche Forschungsgemeinschaft (DFG) for financial support of the investigations.

References

Anderson, R. N., H. O'Malley, and R. L. Newmark, Use of geophysical logs for quantitative determination of fracturing, alteration and lithostratigraphy in the upper oceanic crust, Deep Sea Drilling Project, Holes 504B and 556, *Initial Rep. Deep See Drill. Proj., 83*, 443-478, 1985.

Anderson, R. N., J. C. Alt, J. Malpas, M. A. Lovell, P. K. Harvey, and E. L. Pratson, Geochemical well logging in basalts: The palisades sill and the oceanic crust of hole 504B, *J. Geophys. Res., 90*, 9265-9292, 1990.

Archi, G. E., Introduction to petrophysics of reservoir rocks, *Bull. Am. Assoc. Pet. Geol., 34* (5), 943-961, 1950.

Backhaus, K., B. Erichson, W. Plinke, C. Schuchard-Ficher, and R. Weiber, *Multivariate Analysenmethoden*, 404 pp., Springer-Verlag, New York, 1987.

Berckhemer, H., et al., Petrophysical properties of the 9-km-deep crustal section at KTB, *J. Geophys. Res.*, this issue.

Borm, G., B. Engeser, B. Hoffers, H. K. Kutter, and C. Lempp, Borehole instabilities in the KTB main borehole, *J. Geophys. Res.*, this issue.

Bram, K., and J. K. Draxler (Eds.), Grundlagenforschung und Bohrlochgeophysik: Bohrlochmessungen in der KTB-Oberpfalz HB, Intervall 1720.0-4512.0 m, *KTB Rep. 92-1*, Niedersächsisches Landesamt für Bodenforsch., Hannover, Germany, 1992.

Bram, K., and J. K. Draxler (Eds.), Basic research and borehole geophysics: borehole logging in the KTB-Oberpfalz HB, interval 4512.0- 6018.0 m, *KTB Rep. 93-1*, Niedersächsisches Landesamt für Bodenforsch., Hannover, Germany, 1993.

Bram, K., and J. K. Draxler (Eds.), Basic research and borehole geophysics (final report): borehole logging in the KTB-Oberpfalz HB, interval 6013.5-9101.0 m., *KTB Rep. 94-1*, Niedersächsisches Landesamt für Bodenforsch., Hannover, Germany, 1994.

Bram, K., J. K. Draxler, and G. Zoth (Eds.), Grundlagenforschung und Bohrlochgeophysik: Bohrlochmessungen in der KTB-Oberpfalz HB, Intervall 0-1720.0 m, *KTB Rep. 91-2*, Niedersächsisches Landesamt für Bodenforsch., Hannover, Germany, 1991.

Broglia, C., and D. Moos, In situ structure and properties of 110 Ma crust from geophysical logs in DSDP Hole 418A, *Proc. Ocean Drill. Program, Sci. Results., 102*, 29-47, 1988.

Cooley, W. W., and P. R. Lohnes, *Multivariate Data Analysis*, 364 pp., John Wiley, New York, 1971.

Daniels, J. J., J. H. Scott, and G. R. Olhoeft, Interpretation of core and well log physical property data from drill hole UPH-3, Stephenson County, Illinois, *J. Geophys. Res., 88* (B9), 7346-7354, 1983.

Draxler, J. K. (Ed.), Grundlagenforschung und Bohrlochgeophysik: Bohrlochmessungen in der KTB-Oberpfalz VB, *KTB Rep. 90-1*, Niedersächsisches Landesamt für Bodenforsch., Hannover, Germany,1990.

Duyster, J., et al., The lithological profile of the KTB Hauptbohrung 6000-7220 m: Report of the Field Laboratory, *KTB Rep. 93-2*, pp. 19-63, Niedersächsisches Landesamt für Bodenforsch., Hannover, Germany,1993.

Duyster, J., A. Grawinkel, and A. Kontny, Petrographic and structural characterization, *KTB Rep. 95-2*, pp. B1-B80, Niedersächsisches Landesamt für Bodenforsch., Hannover, Germany,1995.

Ellis, D. V., *Well Logging for Earth Scientists*, 532 pp., Elsevier, New York, 1987.

Franke, W., The geological framework of the KTB drill site, Oberpfalz, in *The German Continental Drilling Program (KTB)*, edited by R. Emmermann and J. Wohlenberg, pp. 37-54, Springer-Verlag, New York, 1989.

Gatto, H., Logkorrekturen für Bohrlocheinflüsse, *KTB Rep. 92-1*, pp. 215-217, Niedersächsisches Landesamt für Bodenforsch., Hannover, Germany, 1992.

Gatto, H., Determination of elements through geochemical logging in crystalline rocks of the KTB-Oberpfalz HB, *KTB Rep. 93-1*, pp. 251-265, Niedersächsisches Landesamt für Bodenforsch., Hannover, Germany,1993.

Godizart, G., N. Gleiss, J. Hansmann, H. Häussinger, S. Keyssner, J. Kohl, an M. Lapp, Tiefbohrung KTB-Oberpfalz HB, Ergebnisse der geowissenschaftlichen Bohrungsbearbeitung im KTB-Feldlabor (Windischeschenbach), Teufenbereich von 0 bis 1720 m: Geologie, *KTB Rep. 91-3*, pp. B1-B89, Niedersächsisches Landesamt für Bodenforsch., Hannover, Germany,1991.

Goldberg, D., C. Broglia, and K. Becker, Fracturing, alteration, and permeability: In-situ properties in Hole 735B, *Proc. Ocean Drill. Program, Sci. Results, 118*, 261-268, 1991.

Grau, J. A., and J. S. Schweitzer, Elemental concentrations from thermal neutron capture gamma-ray spectra in geological formations, *Nucl. Geophys., 3* (1), 1-9, 1989.

Harjes, H. P., et al., Origin and nature of crustal reflections: Results from integrated seimic measurements at the KTB superdeep drilling site, *J. Geophys. Res.*, this issue.

Harms, U., G. Hirschmann, S. Lich, R. Pechnig, and H. de Wall, Gneisses of the KTB Vorbohrung and Hauptbohrung, I, Lithological units, subdivision and correlation, *KTB Rep. 93-2*, pp. 67-78, Niedersächsisches Landesamt für Bodenforsch., Hannover, Germany, 1993.

Harms, U. and G. Godizart, Formation of metabasic rocks: geochemical interpretation of core and cuttings data, *KTB Rep. 93-2*, pp. 67-78, Niedersächsisches Landesamt für Bodenforsch., Hannover, Germany, 1993.

Haverkamp, S., EFA-LOG - Rekonstruktion kristalliner Lithologie anhand von bohrlochgeophysikalischen Messungen für die Bohrungen Urach 3 und KTB-Oberpfalz VB, doctor thesis, 213 pp., Rhein. Westf. Tech. Hochschule, Aachen, Germany, 1991.

Haverkamp, S. and J. Wohlenberg, EFA-LOG - Rekonstruktion kristalliner Lithologie anhand von bohrlochgeophysikalischen Messungen für die Bohrungen Urach 3 und KTB-Oberpfalz VB, *KTB Rep. 91-4*, 213 pp., Niedersächsisches Landesamt für Bodenforsch., Hannover, Germany, 1991.

Hirschmann, G., and M. Lapp, Evaluation of the structural geology of the KTB Hauptbohrung, *KTB Rep. 94-1*, pp. 285-308, Niedersächsisches Landesamt für Bodenforsch., Hannover, Germany, 1994.

Hirschmann, G., S. Lich, and H. de Wall H., KTB Oberpfalz - einige Ergebnisse der geowissenschaftlichen Bearbeitung. *Zentrabl. Geol. Paläontol., 7/8*, 861-873, 1994.

Huenges, E., C. Bücker, K. E. Wolter, J. Wienand, A. Rauen, and E. Lippmann, Deep Drilling KTB Oberpfalz VB - Results of the geoscientific proceedings in the KTB-laboratory; depth interval: 1709-2500 m, *KTB Rep. 89-2*, pp. D1-D83, Niedersächsisches Landesamt für Bodenforsch., Hannover, Germany, 1989.

Huenges, E., B. Engeser, J. Erzinger, W. Kessels, and J. Kück, The permeable crust: Geohydraulic properties down to 9100 m depth, *J. Geophys. Res.*, this issue.

Kendall, M., and A. Stuart, *The Advanced Theory of Statistics*, Vol. 3, 585 pp., Charles Griffin, London, 1976.

Kessels, W., and J. Kück, Hydraulic communication in crystalline rocks between the two boreholes of the Continental Deep Drilling Programme in Germany, *Int. J. Rock Mech. Min. Sci. Geomech.*, *32*(1), 37-47, 1995.

Lich, S., J. Duyster, G. Godizart, S. Keyssner, and H. de Wall, German Continental Deep Drilling Program (KTB), -Geological survey of the Hauptbohrung 0-6000 m: B. Geologie, *KTB Rep. 92-2*, pp. B1-B42, Niedersächsisches Landesamt für Bodenforsch., Hannover, Germany, 1992.

Machon, L., Geochemistry/fluid analysis, *KTB Rep. 95-2*, pp. C1-C28, Niedersächsisches Landesamt für Bodenforsch., Hannover, Germany, 1995.

Möller, P., *Anorganische Geochemie*, 326 pp., Springer-Verlag, New York, 1986.

Moos, D., Petrophysical results from logging in DSDP Hole 395A, ODP Leg 109, *Proc. Ocean Drill. Program Sci. Results*, *109*, 237-253, 1990.

Nelson, P. H., and D. Johnston, Geophysical and geochemical logs from a copper oxide deposit, Santa Cruz Project, Casa Grande, Arizona, *Geophysics*, *59*(12), 1827-1838, 1994.

O'Brien, P. J., J. Duyster, B. Grauert, W. Schreyer, B. Stöckert, and K. Weber, Crustal evolution of the KTB drill site: From the oldest relics to the late Hercynian granites, *J. Geophys. Res.*, this issue.

Paillet, F. L., Use of geophysical well logs in evaluating crystalline rocks for siting of radioactive-waste repositories, *Log Anal.*, *72*(2), 85-107, 1991.

Pechnig, R., Die Lithologie der Kontinentalen Tiefbohrung KTB-HB - eine Interpretation geophysikalischer Logs (EFA-LOG 280-7140 m), *Aachener Geowiss. Beitr. 11*, 143 pp., Augustinus, Aachen, Germany, 1996.

Pechnig, R., and U. Harms, U., Petrogenetic Logging in Crystalline Rocks.- paper presented at the VIIth International Symposium on the Observation of the Continental Crust Through Drilling, sponsored by DOE, NSF, USGS, Santa Fe, N.M., 1994.

Pechnig, R., and J. Wohlenberg, EFA-LOG - The upper 3 km of the KTB-Hauptbohrung, *KTB Rep. 93-1*, pp. 265-280, Niedersächsisches Landesamt für Bodenforsch., Hannover, Germany, 1992.

Pechnig, R., and J. Wohlenberg, EFA-LOG - Reconstruction of lithology by log interpretation - hole to hole correlation in KTB, *KTB Rep. 93-2*, pp. 381-384, Niedersächsisches Landesamt für Bodenforsch., Hannover, Germany, 1993.

Pezard, P.A., Electrical properties of mid-ocean ridge basalt and implications for the structure of the upper oceanic crust in Hole 504B, *J. Geophys. Res.*, *95*, 9237-9292, 1990.

Pratson, E. L., R. N. Anderson, R. E. Dove, M. Lyle, L. T. Silver, E. J. James, and B. W. Chappell, Geochemical logging in the Cajon Pass drill hole and a new, oxide, igneous rock classification sheme, *J. Geophys. Res.*, *97*, 5167-5180, 1992.

Röhr, C., J. Kohl, W. Hacker, S. Keyssner, H. Müller, J. Sigmund, A. Stroh, and G. Zulauf, Results of scientific investigation in the KTB field laboratory, part B: Geology, *KTB Rep. 90-8*, pp. B5-B53, Niedersächsisches Landesamt für Bodenforsch., Hannover, Germany, 1990.

Sattel, G., FACIOLOG - Anwendung eines Programmsystems zur Charakterisierung der Kristallin-Lithologie, *NAGRA Inf.*, *8*(1), 18-24, 1986.

Schweitzer, J. S., D. V. Ellis, J. A. Grau, and R. C. Hertzog, Elemental concentrations from gamma-ray spectroscopy logs, *Nucl. Geophys.*, *2*(3), 175-181, 1988.

Serra, O., *Fundamentals of Well-Log Interpretation*, Vol. 1, Elsevier, Amsterdam, 1984.

Serra, O., *Fundamentals of Well-Log Interpretation*, Vol. 2, Elsevier, Amsterdam, 1986.

Siegesmund, S., A. Vollbrecht, T. Chlupac, G. Nover, H. Dürrast, J. Müller, and K. Weber, Fabric-controlled anisotropy of petrophysical properties observed in KTB core samples, *Sci. Drill.*, *4*, 31-54, 1993.

Simon, K. and J. Hoefs, O, H isotopes of rocks and minerals: Crustal profile and fluid evolution, *KTB Rep. 93-2*, pp. 447-450, Niedersächsisches Landesamt für Bodenforsch., Hannover, Germany, 1993.

Stroh, A., J. Hansmann, H. J. Heinschild, K. D. Homann, M. Tapfer, M. Wittenbecher, and M. Zimmer, Drill hole KTB Oberpfalz VB, geoscientific investigations in the KTB Field Laboratory, geochemistry, Depth interval 0-4000.1 m, *KTB Rep. 90-8*, pp. C1-C37, Niedersächsisches Landesamt für Bodenforsch., Hannover, Germany, 1990.

Tetzlaff, D. M., E. Rodriguez, and R. L. Anderson, Estimating facies and petrophysical parameters from integrated well data, paper presented at the SPWLA Log Anal. Software Eval. Rev., London, England, 1989.

Umsonst, Th., J. Lauterjung, T. T. Viet, and T. Wöhrl, Technical aspects and sampling procedures at the KTB-Hauptbohrung, *KTB Rep. 95-2*, pp. A1-A11, Niedersächsisches Landesamt für Bodenforsch., Hannover, Germany, 1995.

Weber, K., Observation on the ductile deformation path of the paragneisses of the KTB pilot hole, *KTB Rep. 90-8*, pp. J3-J19, Niedersächsisches Landesamt für Bodenforsch., Hannover, Germany, 1990.

Weber K. and A. Vollbrecht, The crustal structure at the KTB drill site, Oberpfalz, in *The German Continental Drilling Program (KTB)*, edited by R. Emmermann, and J. Wohlenberg, pp. 5-36, Springer Verlag, New York, 1989.

Wimmenauer, W., Das prävariskische Kristallin im Schwarzwald, *Fortschr. Mineral.*, *62*(2), 69-86, 1984.

Zimmermann G., Integrierte Auswertung von Bohrlochmessungen der Kontinentalen Tiefbohrung (KTB) mit Verfahren der Multivariaten Statistik, doctor thesis, Tech. Univ. Berlin, Germany, 1991.

Zimmermann, G., C. Bücker, M. Melchert, and T. Wöhrl, Comparison of gamma-ray log and core measurements in the KTB Pilot Well- A method to estimate the depth offset between logging and coring, *Sci. Drill.*, *3*, pp. 1-5, 1992a.

Zimmermann G., H. Burkhardt, M. Melchert, Estimation of porosity in crystalline rock by a multivariate statistical approach, *Sci. Drill.*, *3*, pp. 27-35, 1992b.

Zulauf, G., Zur spät- bis postvariszischen Krustenentwicklung in der nördlichen Oberpfalz. *KTB Rep. 91-3*, pp. 41-62, Niedersächsisches Landesamt für Bodenforsch., Hannover, Germany, 1991.

H. Burkhardt and G. Zimmermann, Institut für Angewandte Geophysik, Technische Universität Berlin, Ackerstrasse 71-76, D-13355 Berlin, Germany. (e-mail: zimm1638@geoph035.bg.tu-berlin.de)

S. Haverkamp, R. Pechnig, and J. Wohlenberg, Lehr- und Forschungsgebiet für Angewandte Geophysik, RWTH Aachen, Lochnerstrasse 4-20, D-52056 Aachen, Germany. (e-mail: renate@sun.geophac.rwth-aachen.de)

(Received February 2, 1996; revised November 22, 1996; accepted December 4, 1996.)